A Comprehensive Chemical Model for the Splitting of CO_2 in Non-Equilibrium Plasmas

Peter Koelman*[1], Stijn Heijkers[2], Samaneh Tadayon Mousavi[1], Wouter Graef[3], Diana Mihailova[3], Tomas Kozak[4], Annemie Bogaerts[2] and Jan van Dijk[1]

[1]Eindhoven University of Technology, Department of Applied Physics, P.O. Box 513, 5600 MB Eindhoven, The Netherlands.
p.m.j.koelman@tue.nl
[2]University of Antwerp, Department Chemistry, PLASMANT, Campus Drie Eiken, Universiteitsplein 1, 2610 Antwerpen-Wilrijk, Belgium.
[3]Plasma Matters B.V., Den Dolech 2 Flux 3.112, 5612 AZ Eindhoven, The Netherlands.
[4]Department of Physics and NTIS - European Centre of Excellence, University of West Bohemia, Univerzitni 8, 30614 Plzen, Czech Republic.

Keywords. CO_2, Modeling, Non-Equilibrium, Verification, Vibrational modes

Abstract

In this work an extensive chemical model is presented for a CO_2 plasma that is relevant for the production of 'solar fuels'. It consists of 72 species and 5732 reactions. It is based on species definitions and reaction rate coefficients from previous literature, which have been rigorously reviewed, and is augmented with reaction rate coefficients that are obtained

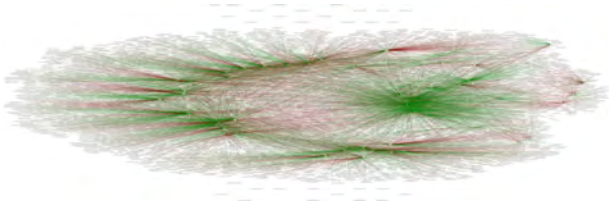

from the application of scaling laws. The input data set, which is suitable for usage with the plasma simulation software Plasimo (see `https://plasimo.phys.tue.nl/`), has been made available in human-readable electronic form on the publisher's website[1]. The correctness of this implementation of the model has been established by realizing an independent ZDPlasKin-compatible implementation (`http://www.zdplaskin.laplace.univ-tlse.fr/`), setting up equivalent physical models and verifying that the results agree. Results of these 'global models' are presented for a typical case study, a cylindrical DBD plasma reactor with pulsed power input.

1 Introduction

Fossil fuels have the advantage of a high energy density and the fact that an extensive transport infrastructure is available. These facts underly the more recent interest in *solar fuels*, in which molecules such as CH_4 are produced from CO_2 using renewable energy sources in an inverse combustion reaction.

In order to produce such fuels from CO_2, the molecule first needs to be dissociated to obtain CO[1;2]. After dissociation, the next step can be to isolate CO from the produced oxygen species using membranes[3;4]. This way the backward reaction of CO to CO_2 is

[1]For the duration of the review period, these files are available on the website `http://epgmod.phys.tue.nl/~jan/CO2`. Please use username 'referee' and password 'co2data'.

avoided. The isolated CO can then be transformed into fuels by combining water gas shift and methanation.

The required energy for direct dissociation of CO_2 from the ground state is $5.5\,\text{eV}$ per molecule. In[2] it is shown that this can be done with a maximum energy efficiency of around $45\,\%$. The CO_2 molecule has, however, three vibrational modes which can be used for a more energy efficient way of dissociation. In previous works it is shown that these vibrational modes provide an energy efficient pathway to dissociation, with an energy efficiency up to $80\,\%$[1;2;5;6]. The asymmetric vibrational mode is shown to be the most important channel for dissociation[2;7]. In the work of Aerts *et al.*[5], an extensive CO_2 chemistry set is presented, which contains 25 species and 205 reactions. The authors validated their results with experimental data obtained by Cenian *et al.*[8]. Later that chemistry was extended by Kozak *et al.*[6;9], mostly by adding the vibrational levels of the asymmetric mode of CO_2. Their chemistry consists of 72 species and several thousands of reactions.

The results in[6] are obtained using the simulation package Global_kin[10], in which spatial dimensions are not resolved, but only the variation of species densities over time are calculated. In this work we will refer to this type of models as Global Models. The results in[6] show that the high vibrational states of CO_2 get significantly populated in a microwave plasma, which is essential for energy efficient dissociation via the vibrational states[2].

The chemistry which is presented in[6] is also at the base of other works[11;12;13]. Implementing such a large model can be challenging. First attempts to implement the chemistry in our own model resulted in significantly different results. This indicates the challenge to

correctly implement a complex chemistry in a new model and stresses the importance of input data verification.

For that reason a verification study is presented in the present paper. Firstly, the chemistry in[6] is subjected to an extensive review study. Secondly, the reviewed chemistry is implemented independently in two Global Models: the Global Model[14] that is part of the PLASIMO plasma modeling framework[15] and ZDPlaskin[16]. Firstly, the two models have been subjected to a code-to-code verification using specially constructed cases. After that the correctness of the input data sets has been established by a comparison of results.

In section 2 the mathematics behind Global Models is introduced. This is followed by a discussion of the implementations of such models in PLASIMO and ZDPlaskin. Next, various scaling laws will be introduced. These are used to obtain reaction data if vibrationally or electronically excited species are considered. In section 3 the species that are considered in this work are presented. This is followed by an extensive review of the literature data that are at the basis of the present model. Various mistakes, ambiguities and inaccurate citations in previous works will be identified and discussed. Section 4 starts with results of basic correctness testing of the PLASIMO and ZDPlaskin codes. That discussion is followed by results of these codes for a typical case study of the CO_2 model, a cylindrical DBD plasma reactor with pulsed power input.

2 Model

Fluid models are based on solving moments of the Boltzmann equation. The mass balance equation is the zeroth order moment of the Boltzmann equation, and reads

$$\frac{\partial n_s}{\partial t} + \nabla \cdot (n_s \vec{v_s}) = S_{net,s}, \tag{1}$$

where n_s is the density of species, $\vec{v_s}$ the velocity and $S_{net,s}$ the net species source from chemical reactions. Since Global Models are not spatially resolved, an assumption must be made about the transport term in this equation. In the present work we will assume that there is no transport. Then the evolution of the species densities is only due to local source terms and equation (1) reduces to:

$$\frac{\partial n_s}{\partial t} = S_{net,s}. \tag{2}$$

Consider a reaction i, which can be written as:

$$\Sigma_s \alpha_{i,s} X_s \rightarrow \Sigma_s \beta_{i,s} X_s. \tag{3}$$

Here X_s represents species s, $\alpha_{i,s}$ and $\beta_{i,s}$ the stoichiometric coefficients at the left and right hand side of reaction i respectively. For that reaction the source term of equation (2) is given by:

$$S_{net,s} = \sum_{i=1}^{j} (\beta_{i,s} - \alpha_{i,s}) R_i, \tag{4}$$

with j the total number of reactions and R_i the rate of reaction i, given by:

$$R_i = k_i \prod_s n_s^{\alpha_{i,s}}, \tag{5}$$

with k_i the rate coefficient. Rate coefficients can be constants, but can also vary with the gas temperature, electron temperature T_e or the reduced electrical field E/N (the electrical field E over the density of neutral species N). Below we will elaborate on how the rate coefficients are obtained in both models.

PLASIMO

In PLASIMO the rate coefficients are regarded as functions of the electron energy density U_ϵ or the electron temperature. The electron energy density is calculated by solving the electron energy balance, which is given by[14]:

$$\frac{\mathrm{d}U_\epsilon}{\mathrm{d}t} = \mathrm{P} - Q_{elas} - Q_{inelas}, \tag{6}$$

where P is the input power density, Q_{elas} the sink of electron energy density due to elastic collisions and Q_{inelas} the net energy density sink due to inelastic processes. The sinks of electron energy density are calculated as:

$$Q_{elas} = \sum_{i,elas} \frac{3}{2} k_\mathrm{B} (T_e - T_g) \frac{2m_e}{m_s} R_i, \tag{7a}$$

$$Q_{inelas} = \sum_{i,inelas} U_{th,i} R_i, \tag{7b}$$

with $\sum_{i,elas}$ and $\sum_{i,inelas}$ the summation over all elastic and inelastic reactions respectively, $U_{th,i}$ the threshold energy of the reaction i, T_g the gas temperature and m_e/m_s the ratio of electron mass over the mass of the colliding species. The electron temperature can be calculated from $T_e = 2U_\epsilon/(3k_{\mathrm{B}}n_e)$, with n_e the electron density, and k_{B} the Boltzmann constant. For non-Maxwellian plasmas this is taken to be a *definition* of the electron temperature.

In case a rate coefficient needs to be calculated from a cross section, we use the relation

$$k_i = \int_{\epsilon_{th}}^{\infty} \sigma_i(\epsilon) v(\epsilon) f(\epsilon)\, \mathrm{d}\epsilon, \tag{8}$$

with ϵ the energy, $v(\epsilon)$ the velocity of the electrons, $\sigma(\epsilon)_i$ the cross section of collision i, $f(\epsilon)$ the electron energy distribution function (EEDF) and ϵ_{th} the threshold energy for that specific reaction. For elastic collisions the rate coefficients are calculated following[17]:

$$k_i = \frac{\int_0^\infty \epsilon \sigma_i(\epsilon) v(\epsilon) f(\epsilon) d\epsilon}{\int_0^\infty \epsilon f(\epsilon) d\epsilon}. \tag{9}$$

The EEDF is a plasma specific parameter. For sufficiently high degrees of ionization the EEDF can be assumed to be Maxwellian, more generally it has to be calculated with a Boltzmann solver such as BOLSIG+[18]. This tool calculates the EEDF for a set of cross sections, the plasma composition and reduced electric field. The calculated EEDF is then available in the form of a look-up table (LUT).

Equations 8 and 9 show that the product of the cross section and the EEDF is needed in the rate coefficient integral. If both the EEDF and cross section are given in the form of a LUT, the data of at least one LUT needs to be interpolated, assuming the energy data

of both LUTs do not match exactly. In such case the cross sectional data is interpolated to the energy grid of the EEDF LUT. This is done using a linear interpolation, since cross sections do not obey a specific shape.

Extrapolation of cross section LUT data is not needed at low energy sides of the LUTs. Data of cross sections is typically well described around the threshold value of the reaction. At the high energy side of a cross section LUT the extrapolation is linear, with the constraint that the cross section does not go below $0\,\mathrm{m}^2$, which would be un-physical.

For the numerical integration many efficient schemes are available. Some of these schemes put additional constraints on the integrand as well, for example concerning its smoothness. In this work the general-purpose trapezium method is used, since a wide variety of integrand shapes can be expected.

To calculate the evolution of the species densities, the differential equations (2) and (6) are solved. In PLASIMO's Global Model various solvers are available. In this work the ODE Pack LSODA (Livermore Solver for Ordinary Differential Equations)[19] and DVODE (Double Variable-coefficient Ordinary Differential Equation solver)[20] are used. The absolute and relative tolerances of the solvers are set to 1×10^{-8}.

ZDPlasKin

As in PLASIMO, equation (2) is solved in ZDPlasKin as well. ZDPlasKin provides the option to calculate the rate coefficients from cross sections with an in-line version of the Boltzmann solver BOLSIG. For that calculation the reduced electric field is required. As a result, the energy balance of equation (6) does not need to be solved in ZDPlasKin.

Instead, a routine is used that calculates the reduced electric field from the plasma

parameters. Using the Local Field Approximation, the reduced electric field, is calculated according to[21]:

$$\frac{E}{N} = \frac{\sqrt{\frac{2P}{\sigma}}}{n_0}, \tag{10}$$

with P the input power density, σ the plasma conductivity and n_0 the initial electron density. The plasma conductivity is initially calculated according to[21]:

$$\sigma = \frac{e^2 n_e}{m_e \nu_m} \frac{\nu_m^2}{\nu_m^2 + \omega^2}, \tag{11}$$

where e is the elementary charge, n_e the electron density, m_e the electron mass, ν_m the collision frequency and ω the frequency of the electric field. During the simulation, the plasma conductivity is calculated as[21]:

$$\sigma = \frac{e \nu_d n_e}{\left(\frac{E}{N}\right)_{prev} n_0}, \tag{12}$$

with ν_d the electron drift velocity, which is calculated with the in-line Boltzmann solver BOLSIG[18], and $\left(\frac{E}{N}\right)_{prev}$ the reduced field at the previous time step. In ZDPlasKin the DVODE solver is used with both the absolute and relative tolerances set to 1×10^{-8}.

Scaling laws

Rate coefficient data is available for various charge exchange reactions but often only for reactions in which an ionized species reacts with a ground state species. To have an estimate for the rate coefficient for charge exchange with an electronically excited species, it is suggested in[5], and later adopted in[6], to scale the rate coefficient from the ground

state species. The scaling they report is $k = k_0\epsilon_i^2/\epsilon_e^2$, with k_0 the rate coefficient of the reaction which is used for scaling, ϵ_i the ionization potential of the excited species and ϵ_e the electronic excitation threshold. However, later the authors of[5] published an erratum in which they note that this scaling should be[22]:

$$k = k_0 \frac{\epsilon_i^2}{(\epsilon_i - \epsilon_e)^2}. \tag{13}$$

This scaling is used in this work as well. The definition for ϵ_{i} is the ionization potential of the species in the ground state, which is different from the definition in[5;6].

Reactions of vibrational energy exchange between molecules is one of the additions in[6] with respect to[5]. Since there is little rate coefficient data available for energy exchange between vibrationally excited molecules a scaling law is needed for these reactions as well. The SSH (Schwartz, Slawsky, and Herzfeld) theory, which is applicable to transfer of energy between an-harmonic oscillators[23] is used to that end. Here, this theory will be summarized briefly.

For VT reactions (reactions in which a molecule loses vibrational energy which is completely transferred to heat), the rate coefficient $k_{n,n-1}$, with n the vibrational level of the species, is obtained from scaling of the rate coefficient from the first vibrational level to the ground level $k_{1,0}$ according to:

$$k_{n,n-1} = k_{1,0} Z_n \frac{F(\gamma_n)}{F(\gamma_1)}, \tag{14}$$

with

$$Z_n = n\frac{1-x_e}{1-nx_e}, \tag{15}$$

$$F(\gamma_n) = \frac{1}{2}\left[3 - \exp\left(-\frac{1}{2}\gamma_n\right)\right]\exp\left(-\frac{1}{2}\gamma_n\right), \tag{16}$$

where x_e is the an-harmonicity of the molecule. The parameter γ is defined as[23]

$$\gamma_n = \left(\frac{\pi^2\omega_n^2\mu}{2\alpha^2 k_{\mathrm{B}}T}\right)^{1/2}, \tag{17}$$

with $\omega_n = \Delta E/\hbar = (E_n - E_{n-1})/\hbar$ the energy over the reduced Planck constant, μ represents the reduced mass, α a parameter of the exponential repulsive potential between colliding species, k_{B} the Boltzmann constant and T the gas temperature. In[2;7] this expression is rewritten in a form with practical units, as used in[6].

For VV energy transfer reactions (reactions where vibrational energy is transferred from one species to another) the scaling is slightly different. For a collision in which a species in the n^{th} vibrational state transfers energy to a species in the m^{th} vibrational state, the rate coefficient is scaled according to:

$$k_{n,n-1}^{m-1,m} = k_{1,0}^{0,1} Z_n Z_m \frac{F(\gamma_{n,m})}{F(\gamma_{11})}, \tag{18}$$

where $\gamma_{n,m}$ requires the difference in energy for the entire reaction: $\Delta E = E_n + E_{m+1} - E_{n-1} - E_m$. In[6] the absolute value for the gain of energy is used, which is correct but unnecessary since these scaling laws are only used for exothermic reactions[2]. Endothermic reactions are included via detailed balancing of the exothermic reactions.

Cross sections of electron impact excitation are scaled as well, to obtain a cross section for reactions from vibrationally excited states to higher vibrationally excited states. In literature work can be found on calculations of cross sections of electron-vibrational processes of CO and CO_2 [13;24;25;2]. In this work the scaling is done via the Fridman approximation[2]. The cross section σ_{nm} for vibrational excitation from the n^{th} vibrational state to the m^{th} vibrational state relates to the cross section for vibrational excitation from the ground state to the first vibrational state σ_{01} as:

$$\sigma_{nm}(\epsilon) = \sigma_{01}(\epsilon + \Delta\epsilon) \exp\left(-\frac{\alpha(m-n-1)}{1+\beta n}\right), \tag{19}$$

with α a species dependent parameter, which is given in[2] to be 0.5 and 0.6 for CO_2[2] and CO respectively, $\Delta\epsilon = \epsilon_{01} - \epsilon_{mn}$ the difference in energy which has to be overcome in the reaction from vibrational state m to n with respect to the energy barrier which has to be overcome for excitation from the ground state to the first vibrationally excited state. The parameter β is presented in[6] to be 0, which is adopted in this work.

3 Detailed chemical model description

This section presents the input data used in the models. From equations (2) and (5) it is clear that the species properties are required, completed with rate coefficients for each reaction. It is also shown that scaling laws can be used to obtain input data for reactions of which no reaction data is available. For these scaling laws the energy difference of the species is required (see equations (13), (17) and (19)). In this section we present that data.

[2] In[2] the authors report to use this scaling only for the asymmetric vibrational mode of CO_2.

Firstly, the species that have been taken into account are listed with their corresponding energy. Secondly, a detailed exposition and review of the chemistry is provided, based on the chemistry presented in[6].

Species

The species used in this work are listed in table 1, using the notational convention that also appears in[6]. The first column in table 1 contains all the species in their ground state with the corresponding energy obtained from[26]. The second column gives the electronically excited species denoted by the symbol e, followed by a number indicating the different states. The energies are again obtained from[26]. Some states represent, however, the sum of various electronically excited states. For these species the energy is obtained via the cross sectional data. For more details of the electronically excited species we refer to[5].

Species in the electronic ground state but vibrationally excited are given in the third column. The energy corresponding to the vibrational states are calculated via the anharmonic oscillator approximation, as given in various sources[6;27;28]. Vibrationally excited species are indicated with an additional v. In case of vibrational states of CO_2 there are three modes. The species which represent asymmetric vibrationally excited modes of the CO_2 molecule are indicated by CO_2v_i with $i = 1, ..., 21$. The species CO_2v_α with $\alpha = a, ..., d$ represent collections of the two non-asymmetric vibrational modes. See[6] for more details on the vibrational states. Analogously, the vibrational levels of CO and O_2 are given by COv_i and O_2v_i with $i = 1, ..., 10$ for CO and $i = 1, 2, 3$ for O_2, which is in line with[6].

The fourth and fifth column give the positively and negatively charged ions, respec-

Table 1: The species which are included in the model. For the electronically and vibrationally excited states the notation is used as in[6], followed by the corresponding energy. In case the energy is not known, the energy position is marked by -. For vibrationally excited species the energy is not explicitly given. Electronically excited species (second column) are indicated with the addition of e. Vibrationally excited species (third column) are indicted by the added v.

X_s	ϵ(eV)	X_s	ϵ(eV)	X_s	X_s	ϵ(eV)	X_s	ϵ(eV)
CO_2	−4.08	CO_2e_1	2.92	$CO_2v_a..v_d$	CO_2^+	9.70	CO_2^-	−3.45
CO	−1.15	CO_2e_2	6.42	$CO_2v_1..v_{21}$	CO_4^+	-	CO_3^-	−5.1
O_2	0.00	COe_1	5.07	$COv_1..v_{10}$	CO^+	12.86	CO_4^-	−5.3
C_2O	2.97	COe_2	6.75	O_2v_1	$C_2O_2^+$	-	O^-	1.1
C	7.43	COe_3	9.95	O_2v_2	$C_2O_3^+$	-	O_2^-	−0.45
C_2	8.69	COe_4	11.75	O_2v_3	$C_2O_4^+$	-	O_3^-	−0.63
O	2.58	O_2e_1	1.00		C^+	18.69	O_4^-	−0.90
O_3	1.48	O_2e_2	1.60		C_2^+	20.09	e^-	-
					O^+	16.20		
					O_2^+	12.07		
					O_4^+	-		

tively, together with the corresponding energies. For some species no energy data is available, in the table this is indicated with the symbol −. Since those species are not used in the scaling laws, the lack of energy data for these species has no impact on this work.

To be able to apply the VV and VT energy exchange scaling laws to this chemistry (equations (14) and (18)), the species dependent parameter α is needed. To obtain this parameter we follow the work of[6] and[29]. There α is given as $\alpha = 17.5/r_0$, with $r_0 = 3.94$ Å, 3.69 Å and 3.47 Å for CO_2, CO and O_2, respectively.

Reaction reference study

The reactions and corresponding rate coefficients in this work are mostly obtained from[6]. For clarity the reaction identities are unchanged where possible. For the verification of the

reactions and their reaction data, the references in[6] have been subjected to a reference study. Reactions in which the data in this work differ from the data which is presented in[6] are shortly discussed below. In tables A1–A5 the complete chemistry is presented, with their ID number which is used for referencing in the reference study below.

Electron impact ionization and excitation reactions

Table A1 gives a list of the electron impact reactions, together with the corresponding reference. The references refer to the cross sections used in this work, and are presented in the form of a LUT.

- Reaction X6 in[6] describes the dissociative ionization reaction of CO_2 to O_2^+. In[6] this reaction is given with a reference to[30]. From that work we have, however, not been able to find the cross section for this reaction, nor from other sources. From[31] we obtained an expression for the rate coefficient for this reaction, which is: $7.0 \times 10^{-19} T_e^{1/2}(1 + 1.3 \times 10^{-5} T_e) \exp(-1.5 \times 10^5/T_e)$, with the electron temperature in Kelvin. The typical electron temperatures in this work are several eV, so this reaction has a significant rate coefficient. For that reason this reaction is included with the rate coefficient instead of a cross section.

- The dissociation of CO in C and O is included in this work with reaction X20a with a reference to[32]. In[6] this reaction is not reported. This reaction is scaled by lowering the energy of the LUT with the threshold energy for the reaction in case vibrationally excited CO species are considered.

- Reaction X25 is the vibrational excitation of CO. In this work this reaction is scaled

with the Fridman approximation (equation (19)), with $\alpha = 0.6$. This note is omitted in[6], although it was included in the model.

- Reaction X28 in[6] describes the elastic electron impact collision with C_2. In that work a reference is given to[33], which discusses cross sectional data for electron impact collisions with C_xH_y for $y > 0$, $x > 0$, and not for C_2. We have not been able to obtain a cross section for the elastic electron impact reaction with C_2 via that work, nor via other work. Because this reaction is an elastic collision, it has no direct impact on the species evolution. This reaction plays a role only as a sink of electron energy and in the calculation of the EEDF. Since the fraction of C_2 is expected to be small, its role will be small as well. For that reason this reaction is excluded in this work.

- Reactions X39 and X40 describe the electronic excitation of O_2 by electrons. The same cross sections are also used in the case that O_2 is in a vibrationally excited state. This is the same as what is done in[6]. The note in that work which should report this scaling, as it is added for the species CO_2 and CO, is unintentionally omitted.

Electron attachment and recombination reactions

Table A2 lists the rate coefficients for electron attachment and electron-ion recombination. Again, the reactions and corresponding rate coefficients are the same as in[6]. Only those reactions for which we have remarks are listed below.

For reactions in which the third body M is presented, this body represents all possi-

ble neutral species in the plasma. In case the given rate coefficient is explicitly reported for some specific species, only the reported species are considered, including their vibrationally excited states.

- Reaction E1 is used in this work as e^- + $CO_2^+ \rightarrow CO v_1$ + O, which differs from[6] in the vibrational state of the CO species. In[6] a reference to[34] is given, where the CO species is considered to be in the vibrational ground state. The authors of[34], however, do not consider vibrationally excited species at all. In their reference to[35] vibrationally excited species are considered, and this reaction is given with $CO v_1$.

- Reaction E4 is adopted from[6] without verification. The authors refer to[36] for the rate coefficient, which we could not use for verification, nor the references therein.

- The rate coefficient of reaction E8 is adopted from[6], since we have not been able to verify this rate coefficient. The impact of this reaction on the chemistry will be small, since the population of C_2^+ and the given rate coefficient are (expected to be) small. Even if this value would be an over or under estimation, this would not influence the validity of the model results.

- The three body reaction E9 considers the general third body M. In this work a scaling parameter is used, which changes with M as given in[8]. The rate coefficients in[8] are given with a reference to[37] for M = CO_2 and O_2 (which are verified as well). For M = CO the rate coefficient is presented as an estimated value. When omitting this scaling parameter, the rate coefficient of this reaction is slightly overestimated for M = CO or O_2.

- Reaction E10 has a constant rate coefficient which is independent of any plasma parameter. In[6] this reaction has the same rate coefficient as used in this work, but with an additional electron temperature dependence. We have not been able to verify the additional temperature dependence. Since the given electron temperature is in units of eV, and the typical electron temperatures are around 1 eV, the impact of the temperature on the actual rate coefficient will be modest.

  From[38] a reference is found to[39], which neither reports an electron temperature dependence. In[39] the rate coefficient is reported as $k \leq 5 \times 10^{-31}$ cm^6/s. In this work the upper boundary value for the rate coefficient is used.

- The rate coefficient of reaction E14 is adopted from[40]. From this reference the rate coefficient is verified for $\mathrm{M} = \mathrm{O}_2, \mathrm{N}_2$. In this work this rate coefficient is used for all M. With 5.51×10^{-46} m^6/s the rate coefficient of this reaction differs strongly from 1×10^{-40} m^6/s, which is presented in[6] and has not been verified with the given reference.

Neutral interactions

Table A3 lists the reactions and rate coefficients for 15 neutral-neutral reactions with their references, adopted from[6]. With the following items the remarks are presented regarding the reactions or rate coefficients in Table A3. This list of reactions contains three body collisions as well. If the third body M is presented, this body represents all possible neutral species in the plasma. In case the rate coefficient is given for a specific species M, only that species and its vibrationally and electronically excited states are included.

- The rate coefficient of reaction N1 is verified based on[41] that is accessible from the NIST database[42]. The heavy species temperature validity range for this rate coefficient is with $2620\,\mathrm{K}$ to $4470\,\mathrm{K}$ far from the heavy species temperature in this study ($300\,\mathrm{K}$). However, due to the lack of data for this reaction at $300\,\mathrm{K}$, the rate coefficient of[41] is used. Although the rate coefficient of[6] is different from the rate coefficient used in this work, the rate coefficients are both in the same order of magnitude if $T_g = 300\,\mathrm{K}$ is substituted in the expression of the rate coefficients. The rate coefficient in[6] is, however, not verified.

- The rate coefficient for reaction N3 is adopted from[38], which reports an upper limit for the rate coefficient of this reaction as $k \leq 1 \times 10^{-21}$ m^3/s. In this work this value is used as rate coefficient, which is equal to what is done in[6].

- In reaction N4 a scaling parameter is included, which accounts for the third body species M = $\mathrm{CO_2}$, CO and $\mathrm{O_2}$, as suggested in[8]. In[6] the scaling parameter for the third body species M is not reported.

- The rate coefficient of reaction N6 is used as a constant value, as it is in[6]. However, in[31] this rate coefficient is reported as an upper limit of this reaction.

- For reaction N7 the rate coefficient is adopted from[43;26]. This rate coefficient is reported to be obtained at $300\,\mathrm{K}$ and $2 \times 10^4\,\mathrm{Pa}$, which is lower than the pressure considered in this work. In[6] a reference to[8] is given, with a slightly different rate coefficient. This rate coefficient is reported in[8] as well, but not in the references therein.

- The used reference for reaction N9 is a modification on the rate coefficient presented in[31]. In that work the exponential behavior of the rate coefficient is reported as $\exp(2114/T_g)$. However, we expect that this is a typographic mistake, and that this should be $\exp(-2114/T_g)$. This is used in[6] as well.

- For reaction N10 the rate coefficient data is obtained from[44], which originates from experiments. The rate coefficient is 9.51×10^{-17} m^3/s, which is in the same order of magnitude as the rate coefficient reported in[6]: 5×10^{-17} m^3/s.

- The rate coefficient of reaction N12 is obtained from the review paper[45]. This is different from the rate coefficient in[6], which originates from theory.

- The rate coefficient of reaction N14 is obtained from[46], which is reported to be valid at 300 K and atmospheric pressure. This is different from[6], where[40] is used as reference which we could not use to verify the rate coefficient. The rate coefficients are, however, close to each other. For that reason we expect that this difference in chemistry does not have a significant impact on the chemistry.

- For reaction N15 the rate coefficient reported in[47] is used. In[6] a reference to[48] is given, which reports a rate coefficient which depends on M = O or O_2. The reported rate coefficient in[6] is, however, not verified with that work. Substituting $T_g = 300$ K in the rate coefficient in[6] and the one of this work we see that the rate coefficients do not agree exactly, but are in the same order of magnitude.

Ion-Neutral interactions

Table A4 lists the ion-neutral reactions. With the items below the notes on the reactions in that table and their rate coefficients are given, which is based on[6]. Unless explicitly stated, the species M is again applicable to all neutral species. In this list and Table A4 the reactions have the same ID number as the corresponding reactions in[6]. Since a few reactions are not included in this work, while they are present in[6] this results in the appearance in missing numbers. This is, however, intended.

- The rate coefficients of reactions I2 and I3 are included in this work as $90\,\%$ and $10\,\%$ of the total rate coefficient of the collision $\mathrm{O^+}$ + $\mathrm{CO_2}$, which is $k = 9 \times 10^{-16}$ m^3/s[49]. In that same work the reaction of I2 is presented with $k = 9.4 \times 10^{-16}$ m^3/s, which is approximately the same as the rate coefficient for the combined rate coefficient of I2 and I3, reported in that work as well. From that we concluded that the fraction of the rate coefficient which results in $\mathrm{O_2^+}$ is likely to be significantly larger than the fraction which results in $\mathrm{O^+}$. This is different from the assumption made in[31], where the rate coefficients have an equal share over the total rate coefficient: 50-50. As a consequence the rate coefficient of reaction I2 is close to the reported value in[6], but the rate coefficient of reaction I3 is one order of magnitude lower in this work.

- In this work reaction I4 is included with the reaction products $\mathrm{CO^+}$ and CO. In[6] this reaction has two times the reaction product $\mathrm{CO^+}$, which is a typographic mistake. This reaction was intended to be $\mathrm{C^+}$ + $\mathrm{CO_2} \rightarrow \mathrm{CO^+}$ + CO.

- The rate coefficient of reaction I6 scales with the third body M, as presented in[8;50;37].

For M = $\mathrm{CO_2}$ or $\mathrm{O_2}$ the rate coefficients are reported explicitly. For M = CO the rate coefficient is, however, presented in[37] as being an estimated value. In[6] the scaling of the rate coefficient with M is not included.

- For Reaction I7 all M are possible. The rate coefficient is, however, only verified for M=$\mathrm{CO_2}$ or $\mathrm{O_2}$ with references[8;37]. For M=CO this rate coefficient is an estimated value.

- For reactions I10, I16 and I17 the reactions are included for all possible third bodies M. In[38] this reaction is, however, reported only for M=$\mathrm{O_2}$. The choice to apply this reaction for all M is the same as what is done in[6].

- For reactions I26 and I27 the produced species $\mathrm{CO_2}$ is in the vibrationally excited state $\mathrm{CO_2[v_b]}$, which is obtained from[35]. In[6] this reaction is reported with $\mathrm{CO_2}$ in the vibrational ground state, as it is in[34]. In[34] a reference to[35] is given too, but since vibrationally excited species are not included in[34], this reaction is reported with $\mathrm{CO_2}$ in the vibrational ground state. The rate coefficients are reported in[34] as estimated values.

- Reaction I28 is included in this work with $\mathrm{COv_1}$ as one of the resulting species, as suggested in[35]. In[6] this vibrational state is omitted, with the same reason as for reactions I26 and I27. Moreover, the stoichiometry is not correct for reaction I28 in[6], which is a typographic mistake. That reaction was intended as a collision between $\mathrm{CO_2^+}$ + $\mathrm{O_2^-}$.

- The rate coefficient of reaction I39 is used for all third body species M. In[38] this

rate coefficient is, however, reported for M=$\mathrm{CO_2}$. Using this reaction for all M is in line with what is done in[6].

- In reactions I43 and I44 $\mathrm{CO_2v_b}$ is produced, which is adopted from[34]. In[6] this reaction is included with the produced $\mathrm{CO_2}$ in the vibrational ground state, with a reference to[38]. In that work[34] is used as reference, but since vibrationally excited species of $\mathrm{CO_2}$ are not included in[38] the notation of the vibrational state was omitted.

- The rate coefficients of reaction I53 and I54 include the gas temperature dependence, which is found in[40]. In that work the third body is reported to be $\mathrm{O_2}$, while it is used in this work for all M. In[6] this is done as well, but in that work the temperature dependence is omitted. Omitting this temperature dependence while working with $T_g = 300\,\mathrm{K}$ does not influence the resulting rate coefficient. For completeness we, however, report this gas temperature dependence as well.

- The rate coefficient for reaction I56 is verified by references[38;51;40]. In references[51;40], the M is presented as $\mathrm{O_2}$, but in[38] it is generalized to M. For this rate coefficient the same reference is used as given in[6], with the general species M.

- The rate coefficient of reaction I57 is included as $5.3 \times 10^{-16}\,\mathrm{m^3/s}$. This is different from $8 \times 10^{-16}\,\mathrm{m^3/s}$, which is reported in[6], although the reference to[38] is used in[6], like it is in this work. Both rate coefficients are, however, in the same order of magnitude, so the impact will on the chemistry is expected to be small.

- The rate coefficient of reaction I59 is verified via[52], which is a different reference than used in[6]. The rate coefficient itself is equal in[6] and this work.

- The rate coefficient for reaction I62 is verified for $\mathrm{M} = \mathrm{O}_2$. This reaction is, however, applied for all M. This is the same as what is done in[6].

- The rate coefficient for reaction I64 is obtained from[51]. However, in[6] a reference is given to[53], but with that work we could not verify the reported rate coefficient. Nevertheless, both rate coefficients are equal, so there is no change in the chemistry.

- A general expression for three body ion-ion recombination is used for reaction I72, which is obtained from[31] and originates from[54]. The rate coefficient for this reaction in[6] is reported to be obtained from[53], for which we have not been able to verify the rate coefficient. The reported rate coefficients are, however, close to each other for $T_g = 300\,\mathrm{K}$.

- The rate coefficient of reactions I73 and I74 is gas temperature dependent based on the reference[51]. In the work of[6], the rate coefficients are presented as constants. These rate coefficients are only in agreement if we use $T_g = 300\,\mathrm{K}$. For completeness we report the gas temperature dependence as well.

- For the rate coefficient of reaction I76 the general expression for three body ion-ion collisions is used which is obtained from[31]. This is the same as for the rate coefficient of reaction I72.

- The rate coefficient of reaction I77 is obtained from[31]. In that work this reaction is explicitly reported as $\mathrm{M} = \mathrm{O}_2$, which is generalized in this work for all M. If $T_g = 300\,\mathrm{K}$ is substituted in the rate coefficient of this reaction the rate coefficient reported in[6] is obtained for reaction I77 with $\mathrm{M} = \mathrm{O}_2$.

In[6] reaction I77 is covered by reaction I78 for $\mathrm{M} = \mathrm{O}_2$. Reaction I78 in[6] is the general expression which we use in reaction I77, with both the same rate coefficient for $T_g = 300\,\mathrm{K}$. Reaction I77 appears in[6] unintentionally, and was not included in the chemistry in[6].

- The rate coefficients of reactions I79 and I80 are gas temperature dependent. This gas temperature dependence is not reported in[6]. In that work a reference is given to[53] from which we have not been able to verify the rate coefficients. Nevertheless the rate coefficients are in the same order of magnitude as the rate coefficients used in this work for both reactions.

- For reaction I81 a gas temperature dependent rate coefficient is used, which is obtained from[31]. In[6] a constant rate coefficient is used equal to the rate coefficient reported in[31] for $T_g = 300\,\mathrm{K}$.

- The rate coefficient of reaction I82 is obtained from[31]. In that work only the third body $\mathrm{M} = \mathrm{O}_2$ is reported explicitly. In this work the rate coefficient is used for all M.

  In[6] this reaction is included with reaction I83 (referring to the reaction ID in[6]), with the side note that at the right hand side of the reaction the general species M is omitted. Reaction I82 in that work is covered by reaction I83 for $\mathrm{M} = \mathrm{O}_2$, and is included in the list of reactions by accident. This reaction was not included in the models of[6].

- The rate coefficient of reaction I84 has a gas temperature dependence which is obtained from[51]. This temperature dependence is not reported in[6]. The temperature

dependence is $300/T_g$, and omitting this temperature dependence while working with $T_g = 300\,\mathrm{K}$ does not influence the resulting rate coefficient. For completeness we, however, report this temperature dependence as well.

- Reaction I85 has a rate coefficient which is obtained from a general expression for ion-ion recombination from[31]. This is different from the rate coefficient used in[6], which we have not been able to verify, but lies in the same order of magnitude if $T_g = 300\,\mathrm{K}$ is assumed.

- The rate coefficient for reaction I86 is obtained from[51], which is a review paper. In[6] a rate coefficient is used which is obtained from theory, and is one order of magnitude larger than the rate coefficient which is used in this work.

- With reaction I87 a gas temperature dependence of the rate coefficient is given. This temperature dependence is not included in[6], while[51] is the same reference as used in this work. This temperature dependence is $300/T_g$. Omitting this temperature dependence while working with $T_g = 300\,\mathrm{K}$ does not influence the resulting rate coefficient. For completeness we, however, report this temperature dependence as well.

- In reaction I88 a gas temperature dependent rate coefficient is reported, which is obtained from[31]. This is different from the constant rate coefficient which is reported in[6]. In that work a reference to[53] is given, from which we have not been able to verify this rate coefficient. For $T_g = 300\,\mathrm{K}$ the two rate coefficients are, however, in good agreement.

- The rate coefficient of reaction I89 is verified for the case that $\mathrm{M} = \mathrm{CO_2}$ based on the reference[38]. However, in this study M is generalized, with the same rate coefficient for all M. This is also done in[6].

- For reaction I90 the temperature dependent rate coefficient is obtained from[40]. This is different from the rate coefficient reported in[6], which we have not been able to verify. At $T_g = 300\,\mathrm{K}$ the two rate coefficients are, however, close together.

- For reaction I91 a temperature dependent rate coefficient is used, which is obtained from[40]. In[6] this same reference is used, but with an other rate coefficient. The rate coefficient in[6] is verified via[52]. In[40] the reaction is presented as $\mathrm{O_4^+ + O_2 \rightarrow O_2^+ + O_2 + O_2}$ which is generalized in this work with $\mathrm{O_2} = \mathrm{M}$ as reacting species.

Vibrational energy transfer

In Table A5 the vibrational energy transfer reactions are listed for the reactions between the ground state species and the first vibrationally excited states. To obtain the complete set of reactions, scaling laws (14) and (18) are needed, as in[6].

- In this work only single quantum transitions are taken into account. Transitions over multiple quantum numbers have rate coefficients which are several orders of magnitude lower[55], which justifies this choice. This is in line with the work of[6], and added for clarity.

- For VV and VT transitions between the symmetric mode vibrational levels again only single quantum transitions are taken into account as in[6].

Microscopic reversibility

Since the EEDF is non-Maxwellian, reverse reactions of electron impact processes can be included via microscopic reversibility, which is done in[6]. In this work the reverse reactions are not included. For reverse reactions between neutral species, detailed balancing is used in this work. The neutral species energy distribution function is likely to be Maxwellian, which justifies the use of detailed balancing. For vibrational excited species the degeneracy is 1, except for $\mathrm{CO_2v_b}$, $\mathrm{CO_2v_c}$ and $\mathrm{CO_2v_d}$ which have a degeneracy of 3, 3 and 6, respectively. This is the same as what is done in[6], although not explicitly denoted.

Superelastic collisions

For palsmas with high electron temperatures superelastic collisions can be important for decreasing the inelastic vibrational energy losses. In that way a lot of energy can be pumped in the vibrationally excited levels of $\mathrm{CO_2}$. In this work we consider, however, a DBD plasma. For thorse plasmas the electron temperature is low. For that reason superelastic collisions are excluded in this work. For microwave discharges superelastic collisions should be include, since the electron temperatures are significantly higher[24]

4 Illustrative examples

This section contains illustrative examples regarding the verification of the chemistry in PLASIMO and ZDPlasKin. Firstly, the implementation of the scaling laws of equations (14) and (18) are verified, by comparing the rate coefficient data with the available data which is presented in[6], followed by a code-to-code validation study. After presenting the

numerical set-up which is used in this study, a validation of the included chemistry in the models is given, based on the results from PLASIMO and ZDPlasKin. Lastly, the results are presented which are obtained by the completely independent models.

Validation of VV and VT reaction input data

The complexity of the scaling equations (13)–(19) can be challenging. In[6] the rate coefficients are depicted for a set of VV and VT reactions, which we use to verify that the rate coefficients are implemented correctly. For that reason the scaling laws are implemented in the form as presented in section 2. The parameter γ_n is used as presented in equation (17). For the calculations all parameters are included with the precision as given in[6]. The energy is obtained from calculations, which happened in double precision, and is included with the same precision in the calculations. The resulting rate coefficients are presented in Figure 1, for the rate coefficients of reactions V2a, V2b, V2c, V7a, V7b, and the reactions $\mathrm{CO_2v_1}$ + $\mathrm{CO_2v_n} \rightarrow \mathrm{CO_2}$ + $\mathrm{CO_2v_{n+1}}$ and $\mathrm{CO_2v_n}$ + $\mathrm{CO_2v_n} \rightarrow \mathrm{CO_2v_{n-1}}$ + $\mathrm{CO_2v_{n+1}}$. A gas temperature of $300\,\mathrm{K}$ is used to obtain these results. In this figure the rate coefficients as presented in[6] are depicted as well.

The figure shows that the rate coefficients which result from the scaling law for VV and VT energy exchange reactions in this work are close to the rate coefficients which are presented in[6], but not equal. The difference becomes larger for the rate coefficient of reactions if the energy difference in the reaction is larger. To confirm the difference in results can be explained by the value of the parameter γ_n, we did a sensitivity analysis. From that analysis it turned out that rounding off the values of the parameters in γ_n indeed explain the observed differences in the results. Since γ_n is used in an exponential

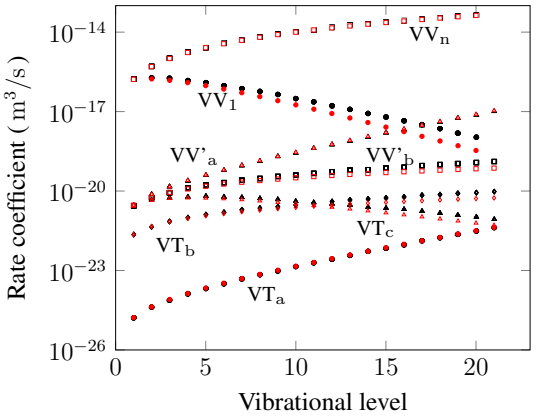

Figure 1: The rate coefficients resulting from the scaling law for VV and VT energy exchange reactions. In red the rate coefficients from this work are depicted. In black the rate coefficients which are presented in[6] are depicted. With the curves the reaction is given, with $\mathrm{VT_A}$, $\mathrm{VT_b}$, $\mathrm{VT_c}$, $\mathrm{VV'_a}$ and $\mathrm{VV'_b}$ representing rate coefficients of reaction 2a, 2b, 2c, 7a and 7b, respectively. $\mathrm{VV_1}$ represents the rate coefficient of reaction $\mathrm{CO_2v_1 + CO_2v_n \rightarrow CO_2 + CO_2v_{n+1}}$, and $\mathrm{VV_n}$ represents $\mathrm{CO_2v_n + CO_2v_n \rightarrow CO_2v_{n-1} + CO_2v_{n+1}}$. The rate coefficients are obtained for a gas temperature of $300\,\mathrm{K}$.

function to obtain the rate coefficients, small differences get magnified in the resulting rate coefficient $k_{n,n-1}$ or $k_{n,n-1}^{m-1,m}$, which is seen best if γ_n is large (thus also for large energy differences).

From this figure and the corresponding analysis we conclude that the scaling law for VV and VT energy exchange reactions (equations (13) - (19)) are implemented correctly in the chemistries in PLASIMO and ZDPlasKin. The differences in the results due to accuracy of the parameters in the scaling laws show that numerical accuracy of parameters is important for the verification of results.

Code-to-code validation

The importance of accuracy underlines that code-to-code validation of the models must be performed, before results of these models can be used for analysis. Such a validation study is done, which includes the definition of universal constants in the models. The use of universal constants in models is at first sight rather trivial, but as with the accuracy of the parameters in the scaling laws this can impact the results significantly. To illustrate, the impact of variations in the precision of the Boltzmann constant k_{B} is considered. The Boltzmann constant typically appears in an exponential function f of the form:

$$f = f(k_{\mathrm{B}}) = \exp(-\epsilon_{th}/(k_{\mathrm{B}}T_e)) \Longrightarrow \frac{k_{\mathrm{B}}}{f}\frac{\partial f}{\partial k_{\mathrm{B}}} = \frac{\epsilon_{th}}{k_{\mathrm{B}}T_e}. \tag{20}$$

Here we see how $\partial f/f$, the relative change in f, changes with a relative change in k_{B}. This means that for a large $\epsilon_{th}/(k_{\mathrm{B}}T_e)$ a small change in $\partial k_{\mathrm{B}}/k_{\mathrm{B}}$ has a big impact on the relative change in f. The impact on the absolute model results will be small (in general), due to the high threshold energy with respect to the electron temperature. The relevant

constants used in the model are obtained from the NIST data-base[56], with the accuracy which is given there.

The ultimate goal is to establish that the input data sets that were developed for PLASIMO and ZDPlasKin are equivalent by setting up equal models and verifying that the results agree. Before we undertook that effort we have carried out some basic correctness tests of the codes themselves. To that end we have developed a two-particle test case for which an analytical solution exists. Consider species densities n_g and n_i, with n_g the ground species density and $n_i = n_e$ the ion density which equals the electron density n_e due to quasi neutrality. These species densities vary due to one reaction, which has a time dependent reaction rate coefficient $k(t)$:

$$\frac{\mathrm{d}n_g}{\mathrm{d}t} = -n_e\, n_g\, k(t), \tag{21}$$

with

$$k(t) = -k_0 \cos(\omega t), \tag{22}$$

and k_0 the amplitude of the rate coefficient and ω the angular frequency. Solving equation (21) this results in the evolution of n_g, which reads:

$$n_g(t) = \frac{N n_0}{(N - n_0) \exp\left(\frac{N k_0}{\omega} \sin(\omega t)\right) + n_0}, \tag{23}$$

where n_0 is the initial density of n_g and $N = n_g + n_i$ the sum of the ion and ground state densities.

In Figure 2 the solution for this equation is shown with a black solid line for $N = 1 \times 10^{25}\,\mathrm{m}^{-3}$, $n_0 = 9 \times 10^{24}\,\mathrm{m}^{-3}$, $\omega = 5000\,\mathrm{s}^{-1}$ and $k_0 = 1 \times 10^{-20}\,\mathrm{m}^3$/s, together with the results obtained with PLASIMO (red markers) and ZDPlasKin (blue markers). The

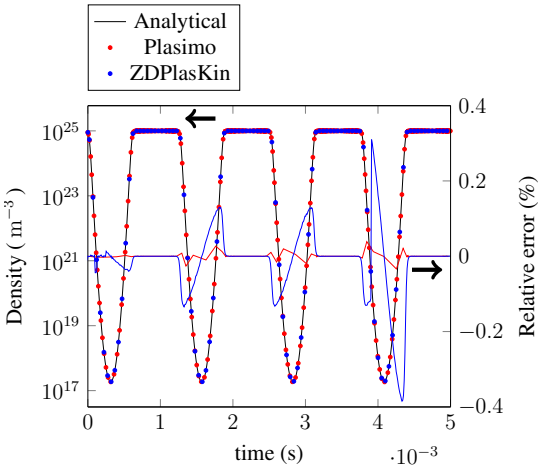

Figure 2: The evolution of n_g as a function of time for a cosine time dependent rate constant. With the black solid line the result of the analytical expression is given. With red and blue markers the result of PLASIMO and ZDPlasKin are presented, respectively. The red and blue solid lines represent the relative difference with the analytical solution for PLASIMO and ZDPlasKin, respectively.

models have run for four full "cycles" of the rate coefficient. In this same figure the relative difference between the results from the models and the analytical result is given as well with the colored solid lines. The red line represents the difference between the analytical result and the result from PLASIMO and the blue line the difference between the analytical result and the result of ZDPlasKin. The relative difference of both models during the first cycle (at $0.6\,\text{ms}$) is in the order of 1×10^{-5} for PLASIMO and 1×10^{-4} for ZDPlasKin. The relative errors accumulate over time to approximately 3×10^{-4} and 4×10^{-3} for PLASIMO and ZDPlasKin, respectively, during the fourth cycle. From these results we conclude that the results obtained by PLASIMO and ZDPlasKin are both in good agreement with the expected result. This justifies the comparison of results between PLASIMO and ZDPlasKin later in this work.

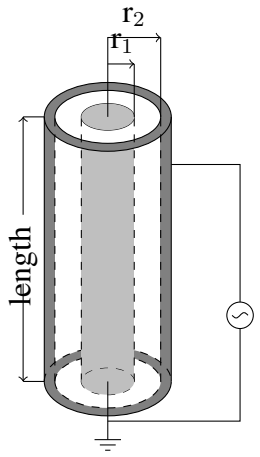

Figure 3: A schematic representation (out of scale) of the set-up as considered in this work. The grounded electrode is positioned at r_1 =11 mm and the powered electrode is wrapped around a dielectric tube at r_2 =13 mm.

Set-up & initial condition

The set-up in this work is the same as in[5] and[6], and presented in Figure 3. The plasma shape is a cylindrical tube with an inner radius of r_1 =11 mm and an outer radius of r_2 =13 mm. The length of the plasma is 90 mm. The outer wall of the reactor is covered on the outside by an electrode which is powered by an external power source. The inner wall of the reactor is defined as the grounded electrode. Initially, the electron temperature is equal to the heavy particle temperature, 300 K. The species densities are in Boltzmann equilibrium[57]:

$$\frac{n_q^B}{g_q} = \frac{n_p^B}{g_p} \exp\left(-\frac{E_{pq}}{k_{\mathrm{B}} T_e}\right), \tag{24}$$

where g_p and g_q are the degeneracy of species p and q, n_p^B and n_q^B are the densities of the corresponding species, and T_e is the electron temperature. The initial electron density is obtained from quasi neutrality.

The input power density is a triangular shaped pulse in time, simulating one micro-discharge of a dielectric barrier discharge. The pulse starts at $0\,\mathrm{ns}$, and rises linearly to $2 \times 10^{11}\,\mathrm{W/m^3}$ in $15\,\mathrm{ns}$, to fall back to $0\,\mathrm{W/m^3}$ at $30\,\mathrm{ns}$. Effectively, this results in a power density deposition of $3000\,\mathrm{W/m^3}$ in one pulse.

Chemistry verification

To validate that both PLASIMO and ZDPlasKin contain the same chemistry, the input data is cross checked for both models. This comparison started with a small chemistry, containing two species and one reaction. Then, stepwise the chemistry was expanded by adding species and reactions, comparing the results between the models at each step and verifying the correct implementation. This resulted in a chemistry which contains 72 species and 5732 reactions. To be able to verify the chemistry based on the results of the models, both models were temporarily modified such that they work exactly the same. Both models solve the equations (2)–(5), with the rate coefficients calculated for an imposed time dependent electron temperature. The results of the models are discussed below for the models containing the complete chemistry.

Following Kozak *et al.*[6], we use the vibrational temperature in the presentation and analysis of the model results. This is defined as:

$$T_{\nu_1} = \frac{E_0 - E_1}{k_\mathrm{B} \log(n_1/n_0)}, \tag{25}$$

where E_1 is the energy of the first asymmetric vibrational level of $\mathrm{CO_2}$, E_0 the energy of the ground state $\mathrm{CO_2}$ species, and n_1 and n_0 the densities corresponding to $\mathrm{CO_2v_1}$ and $\mathrm{CO_2}$, respectively. The impact of rounding off is again clearly visible with the calculation

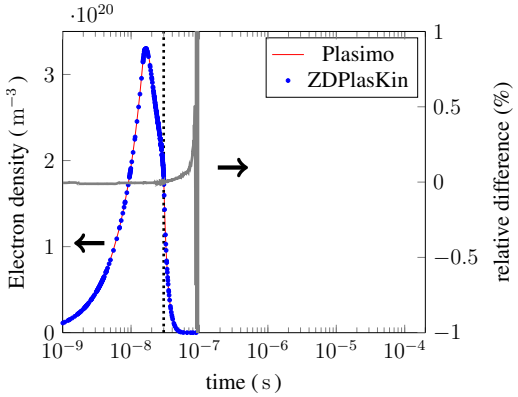

Figure 4: The evolution of the electron density over time for the results from ZDPlasKin (in blue) and PLASIMO (in red). The models are driven by an imposed electron temperature. This electron temperature simulates a power pulse, of which the end is indicated with the vertical dotted line. The difference in results is depicted in gray at the secondary axis of the figure. Both PLASIMO and ZDPlasKin use the DVODE solver, with a relative accuracy of 1×10^{-8}. Since comparison of the results is meaningless for low densities due to underflow problems, the results are only depicted up to 82.9 ns.

of the fraction $(E_0 - E_1)/k_\mathrm{B}$. In[6] this is reported as -3377 K, while our calculation results in -3382.590 K. The impact on the analysis of the results will clearly be small, but in line with the verification issues which have been discussed above we present this result here.

In Figure 4 the evolution of the electron density is given as function of time for the results of PLASIMO (red line) and ZDPlasKin (blue markers). The relative difference between the two models is given with the gray line, given at the secondary y-axis. The vibrational temperature is given in Figure 5, with the results from PLASIMO and ZDPlasKin in red and blue, respectively. The same figure contains a plot of the difference between the two models with a gray line, again with the secondary y-axis. The depicted results of both models are obtained with the DVODE solvers.

The results from both models are in close agreement, as can be seen from Figures 4

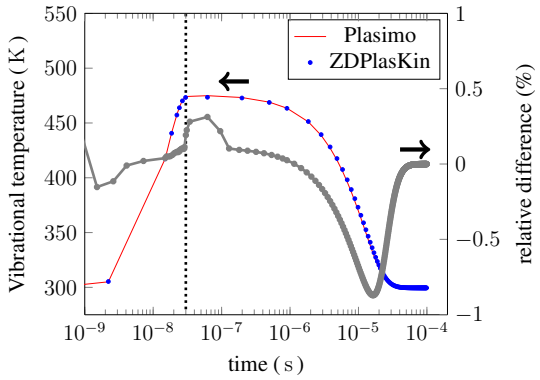

Figure 5: The evolution of the vibrational temperature over time for the results from ZDPlasKin (in blue) and PLASIMO (in red). The models are driven by an imposed electron temperature. This electron temperature simulates a power pulse, of which the end is indicated with the vertical dotted line. The difference in results is depicted in gray at the secondary axis of the figure. Both models use the DVODE solver, with a relative accuracy of 1×10^{-8}.

and 5. The difference in results for the electron density is in the order of $0.1\,\%$ during the power pulse, when the electron density is high. After the power pulse the electron density decreases strongly, resulting in a rising difference between the results of the two models. Due to data underflow, comparison of the results after $8.28 \times 10^{-8}\,\mathrm{s}$ is meaningless. For that reason these results are not included in figure 4 for time exceeding $8.28 \times 10^{-8}\,\mathrm{s}$ (the beginning of the underflow problems is still visible in the figure, indicated by the strong change in relative difference). This same order of difference is also observed when using the LSODA solver in PLASIMO, which indicates that the difference in solvers indeed can be expected from using different solvers[3]. The difference in the vibrational temperature shows a cumulative behavior up to $1 \times 10^{-5}\,\mathrm{s}$. Around that time the vibrational temperature gets close to the relaxation temperature of $300\,\mathrm{K}$, and the difference between the

[3] Although PLASIMO and ZDPlasKin both use the DVODE solver, the implementation of the solver is different in both models. In ZDPlasKin the discriminant is calculated analytically for the solver, while for PLASIMO this is implicitly done by the solver.

models starts to decrease again. Based on the relative difference of less than $1\,\%$ we conclude that the results are in close agreement. The differences are caused by the solvers, which we verified by changing the solver in PLASIMO. From the results in Figures 4 and 5 we conclude that the validated chemistry is the same in both models. With the strategy of stepwise including the chemistry we lowered the possibility of introducing unintended input data.

Results from independent models

Until this point the models are forced to handle the chemistry equally, with an imposed electron temperature evolution as driving input for the chemistry. Now both PLASIMO and ZDPlasKin are used to calculate the evolution of the species as presented in section 2. The input power density is used as presented at the set-up description.

In Figure 6 the vibrational temperature is presented for both models as a function of time, with a logarithmic time axis. In the same figure the electron temperature is depicted at the secondary axis. The results obtained with PLASIMO are depicted in red, and the results from ZDPlasKin in blue, with markers for the vibrational temperature and the dotted lines for the electron temperature. The end of the power pulse is indicated with the black dotted vertical line.

From figure 6 we see that the results of PLASIMO and ZDPlasKin are in close agreement. Both models show a rise in vibrational temperature during the power pulse to $530\,\mathrm{K}$. From the start of the afterglow the population of $\mathrm{CO_2v_1}$ decreases over time, bringing the vibrational temperature down to $300\,\mathrm{K}$ in a timescale of the order $1 \times 10^{-5}\,\mathrm{s}$. The results in electron temperature are also in good agreement. In both trend and magnitude the mod-

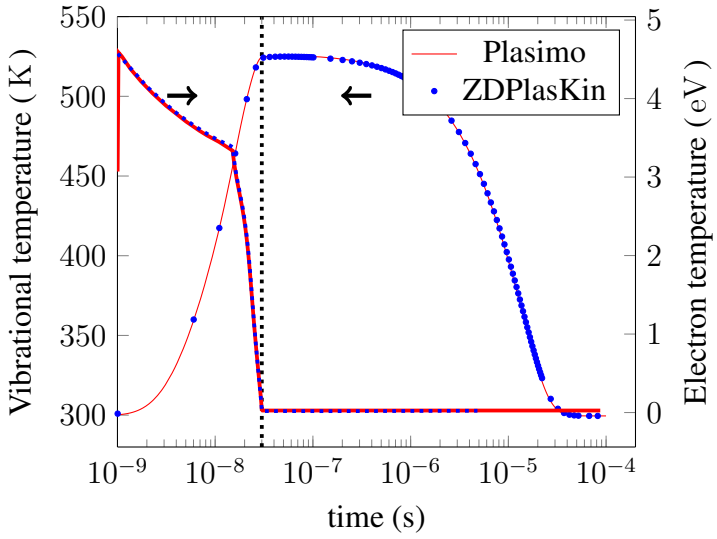

Figure 6: At the primary y-axis the vibrational temperature is given as a function of time, for the results obtained with PLASIMO (red markers) and ZDPlasKin (blue markers). The electron temperature is given at the secondary y-axis, again for PLASIMO (red line) and ZDPlasKin (blue dotted line). The black dotted line indicates the end of the power pulse in time, and the black arrows point to the appropriate axis for the nearest curves.

els obtain the same results. Initially, the electron temperature is at $300\,\mathrm{K}$, and rises early in the pulse to $4.5\,\mathrm{eV}$. This is strongly dependent on the initial conditions of the ion densities, from which the electron density is obtained via detailed balancing. In time scales of the order of $1 \times 10^{-8}\,\mathrm{s}$ electrons are produced. With the rise of the number of electrons the mean energy decreases, resulting in a lowering electron temperature. The electron temperature is at gas temperature shortly after the end of the power pulse, when most of the electron energy is already dissipated out of the system.

The vibrational distribution functions of the asymmetric mode vibrational levels of $\mathrm{CO_2}$ are given in Figure 7 as obtained with PLASIMO (red), and ZDPlasKin (blue). In these results we follow[6], with the results presented at $6\,\mathrm{ns}$, $30\,\mathrm{ns}$, $100\,\mathrm{ns}$ and $1000\,\mathrm{ns}$.

The vibrational distribution functions show that the populations of the vibrational levels are also in close agreement for the results of PLASIMO and ZDPlasKin. At $6\,\mathrm{ns}$ the population of the vibrational levels is rising due to electron impact reactions from the $\mathrm{CO_2}$ species in the vibrational ground state. At the end of the power pulse the population of the vibrational levels is a result of both electron impact reactions and the VV and VT reactions which are given in Table A5.

During the early afterglow (at $100\,\mathrm{ns}$), the electron impact reactions play no role (since the electron temperature is at gas temperature, which we know from Figure 6). The population of the first and second vibrational level is not significantly influenced. The higher vibrational levels are significantly decreased, although the decrease is less strong around the tenth vibrational level. This local increase in density for increasing vibrational level is interesting for the energy efficient dissociation of the $\mathrm{CO_2}$ molecule. At $1000\,\mathrm{ns}$ the depopulation of the vibrational levels is already significant. The vibrational population is

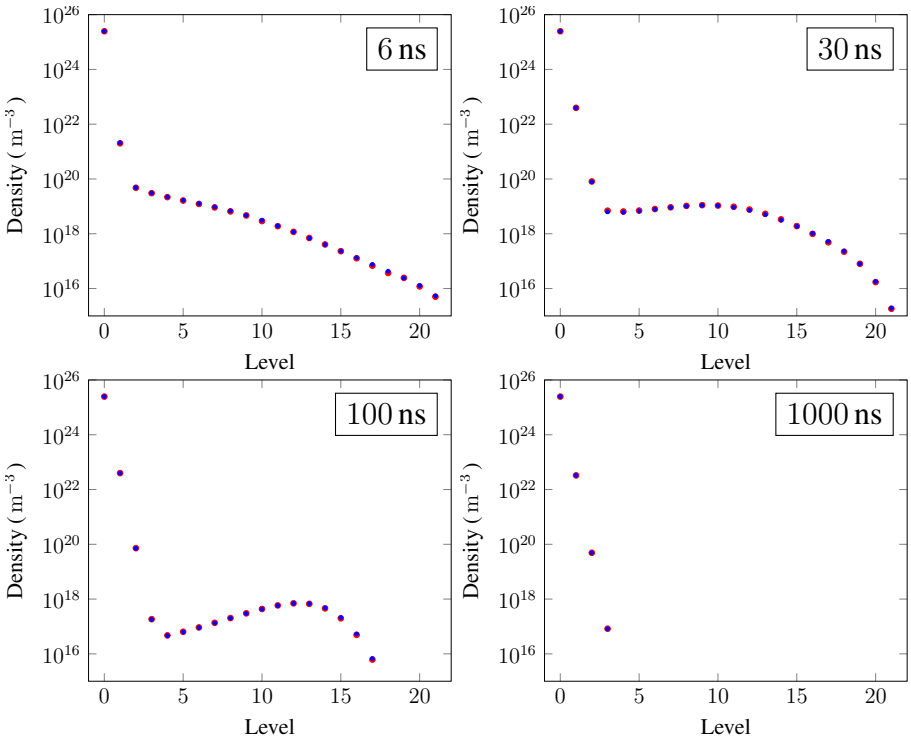

Figure 7: The vibrational distribution function of the vibrational levels from the asymmetric mode of CO_2 at 6 ns, 30 ns, 100 ns and 1000 ns. The results from PLASIMO are given in red, and the results from ZDPlasKin in blue.

not yet completely relaxed (the vibrational temperature is not yet at gas temperature, as is shown in Figure 6), but the local increase in density for increasing vibrational level has already disappeared.

5 Conclusion

In this work we have presented a verification study on the CO_2 chemistry. The global model of PLASIMO and ZDPlasKin have been subjected to a code-to-code verification study. The chemistry which is presented in[6] has been subjected to an extensive review. The reviewed chemistry has been stepwise implemented independently in the two models. By comparison of results the correctness of the implementation of the input data sets has been established. Both models are driven by an imposed electron temperature profile, from which the rate coefficients are calculated in the models. Relative differences in the order of $0.1\,\%$ between the models are observed, which are caused by the solvers that are used by both models. Although underflow of the data limited the time scale for which the results in the electron temperature have been compared, the results show that the chemistry is equally included in both models.

The models of PLASIMO and ZDPlasKin are then used to solve the CO_2 chemistry set completely independently. From a DBD power pulse filament the models are used to calculate the rate coefficients, via the reduced field approximation in the case of ZDPlasKin and the near Maxwellian approximation for PLASIMO. The resulting electron temperature, vibrational temperature, and the vibrational distribution functions of CO_2 are presented. The results from both models are shown to be in close agreement with each

other. The differences between the models are within the differences which can be expected from the models. From this we see that the difference in approximations of the models has no impact on the resulting evolution of the species.

Implementing a chemistry set from well documented articles such as[6;5] is hard. As shown in this article, small implementation differences such as accuracy can influence models. This can make verification of the implemented chemistry even subjective. For that reason the input data-set is distributed in the form of a PLASIMO input file along with this paper. This input file can be used directly to obtain the results presented in this work, or to study more general problems. If using this data set, we kindly request users to refer not only to this work but also to the work of Aerts *et al.* ([5]) and Kozak *et al.* ([6]).

Acknowledgments

This research is supported by the Dutch Technology Foundation STW, which is part of the Netherlands Organization for Scientific Research (NWO), and which is partly funded by the Ministry of Economic Affairs. Furthermore, we acknowledge financial support from the IAP/7 (Inter-university Attraction Pole) program PSI-Physical Chemistry of Plasma-Surface Interactions by the Belgian Federal Office for Science Policy (BELSPO). Part of the calculations were carried out using the Turing HPC infrastructure at the CalcUA core facility of the Universiteit Antwerpen (UAntwerpen), a division of the Flemish Supercomputer Center VSC, funded by the Hercules Foundation, the Flemish Government (department EWI) and the UAntwerpen.

References

[1] V D Rusanov, A A Fridman, and G V Sholin. The physics of a chemically active plasma with nonequilibrium vibrational excitation of molecules. *Soviet Physics Uspekhi*, 24(6):447, 1981.

[2] Alexander Fridman. *Plasma chemistry*. Cambridge University Press, Cambridge New York, 2008.

[3] Lloyd M. Robeson. The upper bound revisited. *Journal of Membrane Science*, 320(12):390 – 400, 2008.

[4] T. Visser, G.H. Koops, and M. Wessling. On the subtle balance between competitive sorption and plasticization effects in asymmetric hollow fiber gas separation membranes. *Journal of Membrane Science*, 252(12):265 – 277, 2005.

[5] R. Aerts, T. Martens, and A. Bogaerts. "influence of vibrational states on CO_2 splitting by dielectric barrier discharges. *The Journal of Physical Chemistry C*, 118(48):28330–28330, 2012.

[6] Tomás Kozák and Annemie Bogaerts. Splitting of CO_2 by vibrational excitation in non-equilibrium plasmas: a reaction kinetics model. *Plasma Sources Science and Technology*, 23(4):045004, 2014.

[7] M. Capitelli, C.M. Ferreira, B.F. Gordiets, and A.I. Osipov. *Plasma Kinetics in Atmospheric Gases*. Springer Series on Atomic, Optical, and Plasma Physics. Springer Berlin Heidelberg, 2000.

[8] A. Cenian, A. Chernukho, V. Borodin, and G. liwiski. Modeling of plasma-chemical reactions in gas mixture of CO_2 lasers i. gas decomposition in pure CO_2 glow discharge. *Contributions to Plasma Physics*, 34(1):25–37, 1994.

[9] T. Kozák and A. Bogaerts. Evaluation of the energy efficiency of CO_2 conversion in microwave discharges using a reaction kinetics model. *Plasma Sources Science Technology*, 24(1):015024, February 2015.

[10] R Dorai. *Modelling of atmospheric pressure plasma processing of gasses and surfaces*. PhD thesis, University of Illinois at Urban-Champaign, 2002.

[11] Kim Peerenboom, Alessandro Parente, Tomas Kozak, Annemie Bogaerts, and Grard Degrez. Dimension reduction of non-equilibrium plasma kinetic models using principal component analysis. *Plasma Sources Science and Technology*, 24(2):025004, 2015.

[12] Stijn Heijkers, Ramses Snoeckx, Tom Kozk, Tiago Silva, Thomas Godfroid, Nikolay Britun, Rony Snyders, and Annemie Bogaerts. CO_2 conversion in a microwave plasma reactor in the presence of N_2: Elucidating the role of vibrational levels. *The Journal of Physical Chemistry C*, 119(23):12815–12828, 2015.

[13] L D Pietanza, G Colonna, G DAmmando, A Laricchiuta, and M Capitelli. Vibrational excitation and dissociation mechanisms of CO_2 under non-equilibrium discharge and post-discharge conditions. *Plasma Sources Science and Technology*, 24(4):042002, 2015.

[14] W A A D Graef. *Zero-dimensional models for plasma chemistry*. PhD thesis, Eindhoven University of Technology, The Netherlands, 2012.

[15] Jan van Dijk, Kim Peerenboom, Manuel Jimenez, Diana Mihailova, and Joost van der Mullen. The plasma modelling toolkit plasimo. *Journal of Physics D: Applied Physics*, 42(19):194012, 2009.

[16] S. Pancheshnyi, B. Eismann, G. J. M. Hagelaar, and L. C. Pitchford. Zdplaskin: A new tool for plasmachemical simulations. 2008.

[17] M. Mitchner and C.H. Kruger. *Partially ionized gases*. Wiley series in plasma physics. Wiley, 1973.

[18] G J M Hagelaar and L C Pitchford. Solving the boltzmann equation to obtain electron transport coefficients and rate coefficients for fluid models. *Plasma Sources Science and Technology*, 14(4):722, 2005.

[19] A.C. Hindmarsh. Toward a systematized collection of ode solvers. *Proc. 10th IMACS Congr. on System Simulation and Scientific Computation*, 1:427432, 1982.

[20] Peter N. Brown and Alan C. Hindmarsh. Reduced storage matrix methods in stiff ODE systems. *Applied Mathematics and Computation*, 31:40–91, May 1989.

[21] M.A. Lieberman and A.J. Lichtenberg. *Principles of Plasma Discharges and Materials Processing*. Wiley, 2005.

[22] Robby Aerts, Tom Martens, and Annemie Bogaerts. Correction to influence of vibrational states on CO_2 splitting by dielectric barrier discharges. *The Journal of Physical Chemistry C*, 118(48):28330–28330, 2014.

[23] G.D. Billing. Vibration-vibration and vibration-translation energy transfer, including multiquantum transitions in atom-diatom and diatom-diatom collisions. In Mario Capitelli, editor, *Nonequilibrium Vibrational Kinetics*, volume 39 of *Topics in Current Physics*, pages 85–112. Springer Berlin Heidelberg, 1986.

[24] L. D. Pietanza, G. Colonna, G. Dapos;Ammando, A. Laricchiuta, and M. Capitelli. Electron energy distribution functions and fractional power transfer in cold and excited CO_2 discharge and post discharge conditions. *Physics of Plasmas*, 23(1), 2016.

[25] V Laporta, C M Cassidy, J Tennyson, and R Celiberto. Electron-impact resonant vibration excitation cross sections and rate coefficients for carbon monoxide. *Plasma Sources Science and Technology*, 21(4):045005, 2012.

[26] P. J. Linstrom and W. G. Mallard, editors. *NIST Chemistry WebBook, NIST Standard Reference Database Number 69*. National Institute of Standards and Technology, Gaithersburg MD, 20899, June 2005.

[27] Isao Suzuki. General anharmonic force constants of carbon dioxide. *Journal of Molecular Spectroscopy*, 25(4):479 – 500, 1968.

[28] G. Herzberg. *Molecular Spectra and Molecular Structure: Spectra of Diatomic molecules*. Prentice-Hall physics series. Van Nostrand, 1950.

[29] R. N. Schwartz, Z. I. Slawsky, and K. F. Herzfeld. Calculation of vibrational relaxation times in gases. *The Journal of Chemical Physics*, 20(10):1591–1599, 1952.

[30] J. J. Lowke, A. V. Phelps, and B. W. Irwin. Predicted electron transport coefficients

and operating characteristics of CO_2N_2he laser mixtures. *Journal of Applied Physics*, 44(10):4664–4671, 1973.

[31] Thomas G. Beuthe and Jen-Shih Chang. Chemical kinetic modelling of non-equilibrium ar-CO_2 thermal plasmas. *Japanese Journal of Applied Physics*, 36(7S):4997, 1997.

[32] James E. Land. Electron scattering cross sections for momentum transfer and inelastic excitation in carbon monoxide. *Journal of Applied Physics*, 49(12):5716–5721, 1978.

[33] R.K. Janev, J.G. Wang, I. Murakami, and T. Kato. Cross sections and rate coefficients for electron-impact ionization of hydrocarbon molecules. 2001.

[34] Hirokazu Hokazono and Haruo Fujimoto. Theoretical analysis of the CO_2 molecule decomposition and contaminants yield in transversely excited atmospheric CO_2 laser discharge. *Journal of Applied Physics*, 62(5):1585–1594, 1987.

[35] R. E. Beverly. Ion aging effects on the dissociative-attachment instability in CO_2 lasers. *Optical and Quantum Electronics*, 14(6):501–513, 1982.

[36] W. Liu and G. A. Victor. Electron energy deposition in carbon monoxide gas. *apj*, 435:909–919, November 1994.

[37] Hirokazu Hokazono, Minoru Obara, Katsumi Midorikawa, and Hideo Tashiro. Theoretical operational life study of the closedcycle transversely excited atmospheric CO_2 laser. *Journal of Applied Physics*, 69(10):6850–6868, 1991.

[38] A. Cenian, A. Chernukho, and V. Borodin. Modeling of plasma-chemical reactions in gas mixture of CO_2 lasers. ii. theoretical model and its verification. *Contributions to Plasma Physics*, 35(3):273–296, 1995.

[39] L. E. Khvorostovskaya and V. A. Yankovsky. Negative ions, ozone, and metastable components in dc oxygen glow discharge. *Contributions to Plasma Physics*, 31(1):71–88, 1991.

[40] I. A. Kossyi, A. Y. Kostinsky, A. A. Matveyev, and V. P. Silakov. Kinetic scheme of the non-equilibrium discharge in nitrogen-oxygen mixtures. *Plasma Sources Science Technology*, 1:207–220, August 1992.

[41] A Eremin, ZIBOROV V. S.and SHUMOVA V. V., VOIKI D., and ROTH P. Formation of o(1d) atoms in thermal decomposition of CO_2. *Kinetics and catalysis*, 38:1, 1997.

[42] J. A. Manion, R. E. Huie, R. D. Levin, D. R. Burgess Jr., V. L. Orkin, W. Tsang, W. S. McGivern, J. W. Hudgens, V. D. Knyazev, D. B. Atkinson, E. Chai, A. M. Tereza, C.-Y. Lin, T. C. Allison, W. G. Mallard, F. Westley, J. T. Herron, R. F. Hampson, and D. H. Frizzell, editors. *NIST Standard Reference Database 17, Version 7.0 (Web Version)*. National Institute of Standards and Technology, Gaithersburg MD, 20899, 2015.

[43] D. Husain and L.J. Kirsch. Reactions of atomic carbon c(23pj) by kinetic absorption spectroscopy in the vacuum ultra-violet. *Trans. Faraday Soc.*, 1971.

[44] W.L. Shackleford, F.N. Mastrup, and W.C. Kreye. Excitation and quenching of CO

fourth positive chemiluminescence due to reactions involving C_2O. *J. Chem. Phys.*, 57, 1972.

[45] R. Atkinson, D.L. Baulch, R.A. Cox, Jr. Hampson, R.F., J.A. Kerr, M.J. Rossi, and J. Troe. Evaluated kinetic and photochemical data for atmospheric chemistry: supplement vi. iupac subcommittee on gas kinetic data evaluation for atmospheric chemistry. *J. Phys. Chem. Ref. Data*, 26:1329 – 1499, 1997.

[46] H. Hippler, R. Rahn, and J. Troe. Temperature and pressure dependence of ozone formation rates in the range 1 - 1000 bar and 90 - 370 K. *The Journal of Chemical Physics*, 93(9):6560–6569, 1990.

[47] W. Tsang and R. F. Hampson. Chemical kinetic data base for combustion chemistry. part i. methane and related compounds. *Journal of Physical and Chemical Reference Data*, 15(3):1087–1279, 1986.

[48] S Hadj-Ziane, B Held, P Pignolet, R Peyrous, and C Coste. Ozone generation in an oxygen-fed wire-to-cylinder ozonizer at atmospheric pressure. *Journal of Physics D: Applied Physics*, 25(4):677, 1992.

[49] D.L. Albritton. "ion-neutral reaction-rate constants measured in flow reactors through 1977. *Atomic Data and Nuclear Data Tables*, 22(1):1–101, 1978.

[50] H Shields, A L S Smith, and B Norris. Negative ion effects in TEA CO_2 lasers. *Journal of Physics D: Applied Physics*, 9(11):1587, 1976.

[51] J T Gudmundsson and E G Thorsteinsson. Oxygen discharges diluted with argon: dissociation processes. *Plasma Sources Science and Technology*, 16(2):399, 2007.

[52] A A Ionin, I V Kochetov, A P Napartovich, and N N Yuryshev. Physics and engineering of singlet delta oxygen production in low-temperature plasma. *Journal of Physics D: Applied Physics*, 40(2):R25, 2007.

[53] B Eliasson, M Hirth, and U Kogelschatz. Ozone synthesis from oxygen in dielectric barrier discharges. *Journal of Physics D: Applied Physics*, 20(11):1421, 1987.

[54] J.S. Chang and S. Masuda. Mechanism of the ozone formations in a near liquid nitrogen temperature medium pressure glow discharge positive column. *Pure and Appl. Chem*, 60(5):645–650, 1988.

[55] Jay A. Blauer and Gary R. Nickerson. *A Survey of Vibrational Relaxation Rate Data for Processes Important to* CO_2-N_2-H_2O *Infrared Plume Radiation*. 1973.

[56] `http://physics.nist.gov/cuu/Constants/`. Accessed: 2016-08-05.

[57] J.A. Bittencourt. *Fundamentals of Plasma Physics*. Springer New York, 2004.

[58] Yukikazu Itikawa. Cross sections for electron collisions with carbon dioxide. *Journal of Physical and Chemical Reference Data*, 31(3):749–767, 2002.

[59] O.J. Orient and S.K. Srivastava. Electron impact ionisation of H_2O, CO, CO_2 and CH_4^+. *J. Phys. B: At. Mol. Phys.*, 20:3923–3936, 1987.

[60] P. C. Cosby. Electronimpact dissociation of carbon monoxide. *The Journal of Chemical Physics*, 98(10):7804–7818, 1993.

[61] A. V. Phelps. Tabulations of collision cross sections and calculated transport and

reaction coefficients for electron collisions with O_2. (28):1–12, 09/01/1985 1985. JILA Pub. 3215.

[62] E. Krishnakumar and S.K. Srivastava. Cross-sections for electron impact ionization of O_2. *International Journal of Mass Spectrometry and Ion Processes*, 113(1):1 – 12, 1992.

[63] Woodall, J., Agndez, M., Markwick-Kemper, A. J., and Millar, T. J. The umist database for astrochemistry 2006. *A&A*, 466(3):1197–1204, 2007.

[64] B Eliasson and U Kogelschatz. Electron impact dissociation in oxygen. *Journal of Physics B: Atomic and Molecular Physics*, 19(8):1241, 1986.

[65] Thomas G. Kreutz, James A. O'Neill, and George W. Flynn. Diode laser absorption probe of vibration-vibration energy transfer in carbon dioxide. *The Journal of Physical Chemistry*, 91(22):5540–5543, 1987.

Table A1: The electron impact ionization and excitation reactions in this model, with the corresponding ID and reference from which the data originates. For the reaction ID is unchanged with respect to[6]. For an added reaction the ID ends with an additional a. Most, but not all, of the reactions are described by a cross section. For reactions which are followed by a star we refer to 3 for a discussion on that reaction or its rate coefficient.

No.	Reaction	Ref.	No.	Reaction	Ref.
X1	$e^- + CO_2 \rightarrow e^- + CO_2$	[30] a	X24	$e^- + CO \rightarrow e^- + CO[e_4]$	[32] a
X2	$e^- + CO_2 \rightarrow e^- + e^- + CO_2^+$	[30] a	X25 *	$e^- + CO \rightarrow e^- + CO[v_1]$	[32] c
X3	$e^- + CO_2 \rightarrow e^- + e^- + CO^+ + O$	[58] b	X26	$e^- + C \rightarrow e^- + C$	[30]
X4	$e^- + CO_2 \rightarrow e^- + e^- + C^+ + O_2$	[58] b	X27	$e^- + C \rightarrow e^-$ +e + C^+	[30]
X5	$e^- + CO_2 \rightarrow e^- + e^- + O^+ + CO$	[58] b	X29	$e^- + C_2 \rightarrow e^- + e^- + C + C$	[33]
X6 *	$e^- + CO_2 \rightarrow e^- + e^- + O_2^+ + C$	[31] d	X30	$e^- + C_2 \rightarrow e^- + e^- + C_2^+$	[33]
X7	$e^- + CO_2 \rightarrow O^- + CO$	[30] b	X31	$e^- + O_2 \rightarrow e^- + O_2$	[61] a
X8	$e^- + CO_2 \rightarrow e^- + CO + O$	[58] b	X32	$e^- + O_2 \rightarrow e^- + O + O$	[58] b
X9	$e^- + CO_2 \rightarrow e^- + CO_2[e_1]$	[30] a	X33	$e^- + O_2 \rightarrow e^- + e^- + O_2^+$	[61] a
X10	$e^- + CO_2 \rightarrow e^- + CO_2[e_2]$	[30] a	X34	$e^- + O_2 \rightarrow e^- + e^- + O + O^+$	[62] b
X11	$e^- + CO_2 \rightarrow e^- + CO_2[v_a]$	[30]	X35	$e^- + O_2 \rightarrow O^- + O$	[61] b
X12	$e^- + CO_2 \rightarrow e^- + CO_2[v_b]$	[30]	X36	$e^- + O_2 \rightarrow e^- + O_2[v_1]$	[61]
X13	$e^- + CO_2 \rightarrow e^- + CO_2[v_c]$	[30]	X37	$e^- + O_2 \rightarrow e^- + O_2[v_2]$	[61]
X14	$e^- + CO_2 \rightarrow e^- + CO_2[v_d]$	[30]	X38	$e^- + O_2 \rightarrow e^- + O_2[v_3]$	[61]
X15	$e^- + CO_2 \rightarrow e^- + CO_2[v_1]$	[30] c	X39 *	$e^- + O_2 \rightarrow e^- + O_2[e_1]$	[61] a
X16	$e^- + CO \rightarrow e^- + CO$	[32] a	X40 *	$e^- + O_2 \rightarrow e^- + O_2[e_2]$	[61] a
X17	$e^- + CO \rightarrow e^- + e^- + CO^+$	[59] a	X41	$e^- + O_3 \rightarrow e^- + O_3$	[30]
X18	$e^- + CO \rightarrow e^- + e^- + C^+ + O$	[59] b	X42	$e^- + O_3 \rightarrow e^- + O_2 + O$	[6]
X19	$e^- + CO \rightarrow e^- + e^- + O^+ + C$	[59] b	X43	$e^- + O_3 \rightarrow e^- + e^- + O_2^+ + O$	[6]
X20	$e^- + CO \rightarrow O^- + C$	[32] b	X44	$e^- + O_3 \rightarrow e^- + O^+ + O^- + O$	[6]
X20a *	$e^- + CO \rightarrow e^- + C + O$	[60] b	X45	$e^- + O_3 \rightarrow O^- + O_2$	[30]
X21	$e^- + CO \rightarrow e^- + CO[e_1]$	[32] a	X46	$e^- + O_3 \rightarrow O_2^- + O$	[30]
X22	$e^- + CO \rightarrow e^- + CO[e_2]$	[32] a	X47	$e^- + O \rightarrow e^- + O$	[30]
X23	$e^- + CO \rightarrow e^- + CO[e_3]$	[32] a	X48	$e^- + O \rightarrow e^- + e^- + O^+$	[30]

[a] The same cross section is used for the vibrationally excited species.
[b] The cross section is modified according to equation (4) of[6] for vibrationally excited species. For electronically excited species the energy data from the LUT is shifted with the difference in energy between the species in the ground state and the electronically excited state. Concequently the threshold energy of the process equals the threshold energy in the (modified) LUT.
[c] The cross section is modified according to equation (4) of[6] for vibrationally excited species.
[d] For this reaction a rate coefficient is used, which reads:
$7.0 \times 10^{-19} T_e (1 + 1.3 \times 10^{-5} T_e) \exp(-1.5 \times 10^5 / T_e)$.

Table A2: Electron attachment and electron-ion recombination reactions. The reported rate coefficients have the units m^3/s or m^6/s, with the gas temperature T_g in K and the electron temperature T_e in eV. For reactions which are followed by a star we refer to 3 for a discussion on that reaction or its rate coefficient.

No.	Reaction	Rate coefficient	Ref
E1 *	$e^- + CO_2^+ \rightarrow CO[v_1] + O$	$2.00 \cdot 10^{-11}\, T_e^{-0.5}\, T_g^{-1}$	[34;35]
E2	$e^- + CO_2^+ \rightarrow C + O_2$	$3.94 \cdot 10^{-13}\, T_e^{-0.4}$	[31]
E3	$e^- + CO_4^+ \rightarrow CO_2 + O_2$	$1.61 \cdot 10^{-13}\, T_e^{-0.5}$	[31]
E4 *	$e^- + CO^+ \rightarrow C + O$	$3.68 \cdot 10^{-14}\, T_e^{-0.55}$	[6]
E5	$e^- + C_2O_2^+ \rightarrow CO + CO$	$4.0 \cdot 10^{-13}\, T_e^{-0.34}$	[38]
E6	$e^- + C_2O_3^+ \rightarrow CO_2 + CO$	$5.4 \cdot 10^{-14}\, T_e^{-0.7}$	[38]
E7	$e^- + C_2O_4^+ \rightarrow CO_2 + CO_2$	$2.0 \cdot 10^{-11}\, T_e^{-0.5}\, T_g^{-1}$	[38]
E8 *	$e^- + C2^+ \rightarrow C + C$	$1.79 \cdot 10^{-14}\, T_e^{-0.5}$	[6]
E9 *	$e^- + O_2 + M \rightarrow O_2^- + M$	$3.0 \cdot 10^{-42} \cdot A$ [a]	[8;35]
E10 *	$e^- + O_3 + M \rightarrow O_3^- + M$	$5.0 \cdot 10^{-43}$	[39]
E11	$e^- + O + M \rightarrow O^- + M$	$1.0 \cdot 10^{-43}$	[8]
E12	$e^- + O_2^+ + M \rightarrow O_2 + M$	$1.0 \cdot 10^{-38}$	[37]
E13	$e^- + O_2^+ \rightarrow O + O$	$6.0 \cdot 10^{-13}\, T_e^{-0.5}\, T_g^{-0.5}$	[34;35]
E14 *	$e^- + O^+ + M \rightarrow O + M$	$2.49 \cdot 10^{-41}\, T_e^{-1.5}$	[38]
E15	$e^- + O_4^+ \rightarrow O_2 + O_2$	$2.25 \cdot 10^{-13}\, T_e^{-0.5}$	[40]

[a] $A = 1$, $2/3$ and $2/3$ for $M = CO_2$, CO and O_2 respectively.

Table A3: The neutral-neutral interactions with the rate coefficients as they are included in the model, in units of m^3/s and m^6/s. The coefficient α originates from[9], where the values are presented as estimates. For reactions which are followed by a star we refer to 3 for a discussion on that reaction or rate coefficient.

No.	Reaction	rate	α	Ref
N1 *	$CO_2 + M \rightarrow CO + O + M$	$1.81 \cdot 10^{-16} \exp(-49000/T_g)$	0.8	[41;42]
N2	$CO_2 + O \rightarrow CO + O_2$	$2.8 \cdot 10^{-17} \exp(-26500/T_g)$	0.5	[31;42;47]
N3 *	$CO_2 + C \rightarrow CO + CO$	$\leq 1.0 \cdot 10^{-21}$		[38]
N4 *	$O + CO + M \rightarrow CO_2 + M$	$8.2 \cdot 10^{-46} \exp(-1510/T_g) \cdot A$ [a]	0.0	[8;42]
N5	$O_2 + CO \rightarrow CO_2 + O$	$4.2 \cdot 10^{-18} \exp(-24000/T_g)$	0.5	[31;42]
N6 *	$O_3 + CO \rightarrow CO_2 + O_2$	$\leq 4.0 \cdot 10^{-31}$		[31;42]
N7 *	$C + CO + M \rightarrow C_2O + M$	$6.31 \cdot 10^{-44}$		[43;42]
N8	$O_2 + C \rightarrow CO + O$	$3.0 \cdot 10^{-17}$		[8;42]
N9 *	$O + C + M \rightarrow CO + M$	$2.14 \cdot 10^{-41} (T_g/300)^{-3.08} \exp(-2114/T_g)$		[31]
N10 *	$O + C_2O \rightarrow CO + CO$	$9.51 \cdot 10^{-17}$		[45]
N11	$O_2 + C_2O \rightarrow CO_2 + CO$	$3.3 \cdot 10^{-19}$		[8]
N12 *	$O + O_3 \rightarrow O_2 + O_2$	$8.0 \cdot 10^{-18} \exp(-2056/T_g)$		[42;45]
N13	$O_3 + M \rightarrow O_2 + O + M$	$4.12 \cdot 10^{-16} \exp(-11430/T_g)$		[31]
N14 *	$O + O_2 + M \rightarrow O_3 + M$	$5.51 \cdot 10^{-46} (T_g/298)^{-2.6}$		[46]
N15 *	$O + O + M \rightarrow O_2 + M$	$5.2 \cdot 10^{-47} \exp(900/T_g)$		[47]

[a] $A = 2, 1, 1$ for $M = CO_2$, O_2 and CO, respectively.

Table A4: The list of ion-neutral and ion-ion reactions and rate coefficients, with T_g the gas temperature in K and T_e the electron temperature in eV. The rate coefficients are in units of m^3/s and m^6/s. The ID corresponding to the reactions is kept the same as in[6]. For reactions which are followed by a star we refer to 3 for a discussion on that reaction or rate coefficient.

No.	Reaction	Rate coefficient	Ref
I1	$O_2^+ + CO_2 + M \rightarrow CO_4^+ + M$	$2.3 \cdot 10^{-41}$	[31]
I2 *	$O^+ + CO_2 \rightarrow O_2^+ + CO$	$8.1 \cdot 10^{-16}$	[31;49]
I3 *	$O^+ + CO_2 \rightarrow CO_2^+ + O$	$9.0 \cdot 10^{-17}$	[31;49]
I4 *	$C^+ + CO_2 \rightarrow CO^+ + CO$	$1.1 \cdot 10^{-15}$	[31;49]
I5	$CO^+ + CO_2 \rightarrow CO_2^+ + CO$	$1.0 \cdot 10^{-15}$	[31;49;8;37]
I6 *	$O^- + CO_2 + M \rightarrow CO_3^- + M$ [a]	$9.0 \cdot 10^{-41}$	[8]
I7 *	$O_2^- + CO_2 + M \rightarrow CO_4^- + M$	$1.0 \cdot 10^{-41}$	[8]
I8	$O_3^- + CO_2 \rightarrow CO_3^- + O_2$	$5.5 \cdot 10^{-16}$	[8;37]
I9	$O_4^- + CO_2 \rightarrow CO_4^- + O_2$	$4.8 \cdot 10^{-16}$	[38]
I10 *	$CO_2^+ + CO_2 + M \rightarrow C_2O_4^+ + M$	$3.0 \cdot 10^{-40}$	[38]
I11	$O^+ + CO \rightarrow CO^+ + O$	$4.9 \cdot 10^{-18}(T_g/300)^{0.5} \exp(-4580/T_g)$	[49]
I12	$O^- + CO \rightarrow CO_2 + e^-$	$5.5 \cdot 10^{-16}$	[31;49]
I13	$CO_3^- + CO \rightarrow CO_2 + CO_2 + e^-$	$5.0 \cdot 10^{-19}$	[34]
I14	$C_2O_3^+ + CO \rightarrow CO_2 + C_2O_2^+$	$1.1 \cdot 10^{-15}$	[38]
I15	$C_2O_4^+ + CO \rightarrow CO_2 + C_2O_3^+$	$9.0 \cdot 10^{-16}$	[38]
I16 *	$C_2O_3^+ + CO + M \rightarrow CO_2 + C_2O_2^+ + M$	$2.6 \cdot 10^{-38}$	[38]
I17 *	$C_2O_4^+ + CO + M \rightarrow CO_2 + C_2O_3^+ + M$	$4.2 \cdot 10^{-38}$	[38]
I18	$C^+ + CO \rightarrow C + CO^+$	$5.0 \cdot 10^{-19}$	[31]
I19	$CO^+ + C \rightarrow CO + C^+$	$1.1 \cdot 10^{-16}$	[63]
I20	$O_2^+ + C \rightarrow CO^+ + O$	$5.2 \cdot 10^{-17}$	[63]
I21	$O_2^+ + C \rightarrow C^+ + O_2$	$5.2 \cdot 10^{-17}$	[63]
I22	$C_2^+ + C \rightarrow C_2 + C^+$	$1.1 \cdot 10^{-16}$	[63]
I23	$CO_2^+ + O \rightarrow O_2^+ + CO$	$1.64 \cdot 10^{-16}$	[63]
I24	$CO_2^+ + O \rightarrow O^+ + CO_2$	$9.62 \cdot 10^{-17}$	[63]
I25	$CO_2^+ + O_2 \rightarrow O_2^+ + CO_2$	$5.3 \cdot 10^{-17}$	[63]
I26 *	$CO_3^- + CO_2^+ \rightarrow CO_2[v_b] + CO_2[v_b] + O$	$5.0 \cdot 10^{-13}$	[35]
I27 *	$CO_4^- + CO_2^+ \rightarrow CO_2[v_b] + CO_2[v_b] + O_2$	$5.0 \cdot 10^{-13}$	[35]
I28 *	$CO_2^+ + O_2^- \rightarrow CO[v1] + O_2 + O$	$6.0 \cdot 10^{-13}$	[35]
I29	$CO^+ + O \rightarrow CO + O^+$	$1.4 \cdot 10^{-16}$	[63]
I30	$CO^+ + O_2 \rightarrow CO + O_2^+$	$1.2 \cdot 10^{-16}$	[63]
I31	$C_2O_2^+ + O_2 \rightarrow CO + CO + O_2^+$	$5.0 \cdot 10^{-18}$	[38]
I32	$C_2O_2^+ + M \rightarrow CO^+ + CO + M$	$1.0 \cdot 10^{-18}$	[38]
I33	$C_2O_2^+ + CO_3^- \rightarrow CO_2 + CO + CO + O$	$5.0 \cdot 10^{-13}$	[38]

[a] Multiplied by 1,3.3,3.3 for M=CO_2, CO, O_2 respectively.

Table A4: Continued.

No.	Reaction	Rate coefficient	Ref
I34	$C_2O_2^+ + CO_4^- \rightarrow CO_2 + CO + CO + O_2$	$5.0 \cdot 10^{-13}$	[38]
I35	$C_2O_2^+ + O_2^- \rightarrow CO + CO + O_2$	$6.0 \cdot 10^{-13}$	[38]
I36	$C_2O_3^+ + CO_3^+ \rightarrow CO_2 + CO_2 + CO + O$	$5.0 \cdot 10^{-13}$	[38]
I37	$C_2O_3^+ + CO_4^- \rightarrow CO_2 + CO_2 + CO + O_2$	$5.0 \cdot 10^{-13}$	[38]
I38	$C_2O_3^+ + O_2^- \rightarrow CO_2 + CO + O_2$	$6.0 \cdot 10^{-13}$	[38]
I39 *	$C_2O_4^+ + M \rightarrow CO_2^+ + CO_2 + M$	$1.0 \cdot 10^{-20}$	[38]
I40	$C_2O_4^+ + CO_3^- \rightarrow CO_2 + CO_2 + CO_2 + O$	$5.0 \cdot 10^{-13}$	[38]
I41	$C_2O_4^+ + CO_4^- \rightarrow CO_2 + CO_2 + CO_2 + O_2$	$5.0 \cdot 10^{-13}$	[38]
I42	$C_2O_4^+ + O_2^- \rightarrow CO_2 + CO_2 + O_2$	$6.0 \cdot 10^{-13}$	[38]
I43 *	$O_2^+ + CO_3^- \rightarrow CO_2[v_b] + O_2 + O$	$3.0 \cdot 10^{-13}$	[34]
I44 *	$O_2^+ + CO_4^- \rightarrow CO_2[v_b] + O_2 + O_2$	$3.0 \cdot 10^{-13}$	[34]
I45	$CO_3^- + O \rightarrow CO_2 + O_2^-$	$8.0 \cdot 10^{-17}$	[34]
I46	$CO_4^- + O \rightarrow CO_3^- + O_2$	$1.1 \cdot 10^{-16}$	[31]
I47	$CO_4^- + O \rightarrow CO_2 + O_2 + O^-$	$1.4 \cdot 10^{-17}$	[31]
I48	$CO_4^- + O \rightarrow CO_2 + O_3^-$	$1.4 \cdot 10^{-17}$	[31]
I49	$CO_4^- + O_3 \rightarrow CO_2 + O_3^- + O_2$	$1.3 \cdot 10^{-16}$	[38]
I50	$C^+ + O_2 \rightarrow CO + O^+$	$4.54 \cdot 10^{-16}$	[63]
I51	$C^+ + O_2 \rightarrow CO^+ + O$	$3.8 \cdot 10^{-16}$	[31]
I52	$O^+ + O_2 \rightarrow O_2^+ + O$	$1.9 \cdot 10^{-17}(300/T_g)^{0.5}$	[31]
I53 *	$O_2^+ + O_2 + M \rightarrow O_4^+ + M$	$2.4 \cdot 10^{-42}(300/T_g)^{3.2}$	[40]
I54 *	$O_2^- + O_2 + M \rightarrow O_4^- + M$	$3.5 \cdot 10^{-43}(300/T_g)$	[40]
I55	$O^- + O_2 \rightarrow O_3 + e^-$	$1.0 \cdot 10^{-18}$	[38]
I56 *	$O^- + O_2 + M \rightarrow O_3^- + M$	$1.1 \cdot 10^{-42}(300/T_g)$	[38;51;40]
I57 *	$O^- + O_3 \rightarrow O + O_3^-$	$5.3 \cdot 10^{-16}$	[38]
I58	$O^- + O_3 \rightarrow O_2 + O_2 + e^-$	$3.0 \cdot 10^{-16}$	[52]
I59 *	$O_2^- + O_3 \rightarrow O_2 + O_3^-$	$4.0 \cdot 10^{-16}$	[52]
I60	$O_3^- + O_3 \rightarrow O_2 + O_2 + O_2 + e^-$	$3.0 \cdot 10^{-16}$	[38]
I61	$O^+ + O_3 \rightarrow O_2^+ + O_2$	$1.0 \cdot 10^{-16}$	[40]
I62 *	$O^+ + O + M \rightarrow O_2^+ + M$	$1.0 \cdot 10^{-41}$	[64]
I63 *	$O^- + O \rightarrow O_2 + e^-$	$2.3 \cdot 10^{-16}$	[51]
I64	$O_2^- + O \rightarrow O_2 + O^-$	$3.31 \cdot 10^{-16}$	[51;40]
I65	$O_2^- + O \rightarrow O_3 + e^-$	$1.5 \cdot 10^{-16}$	[51]
I66	$O_3^- + O \rightarrow O_3 + O^-$	$1.0 \cdot 10^{-19}$	[52]
I67	$O_3^- + O \rightarrow O_2 + O_2 + e^-$	$1.0 \cdot 10^{-19}$	[38]
I68	$O_3^- + O \rightarrow O_2^- + O_2$	$2.5 \cdot 10^{-16}$	[38;39]
I69	$O_4^- + O \rightarrow O_3^- + O_2$	$4.0 \cdot 10^{-16}$	[40]
I70	$O_4^- + O \rightarrow O^- + O_2 + O_2$	$3.0 \cdot 10^{-16}$	[40]
I71	$O_4^+ + O \rightarrow O_2^+ + O_3$	$3.0 \cdot 10^{-16}$	[40]
I72 *	$O_2^- + O^+ + M \rightarrow O_3 + M$	$1.0 \cdot 10^{-37}(300/T_g)^{2.5}$	[31]

Table A4: Continued.

No.	Reaction	Rate coefficient	Ref
I73 *	$O_2^- + O^+ \rightarrow O_2 + O$	$2.7 \cdot 10^{-13}(300/T_g)^{0.5}$	[51]
I74 *	$O_2^- + O_2^+ \rightarrow O_2 + O_2$	$2.01 \cdot 10^{-13}(300/T_g)^{0.5}$	[51]
I75	$O_2^- + O_2^+ \rightarrow O_2 + O + O$	$4.2 \cdot 10^{-13}$	[34]
I76 *	$O_2^- + O_2^+ + M \rightarrow O_2 + O_2 + M$	$1.0 \cdot 10^{-37}(300/T_g)^{2.5}$	[31]
I77 *	$O_2^- + M \rightarrow O_2 + M + e^-$	$2.7 \cdot 10^{-16}(300/T_g)^{-0.5} \exp(-5590/T_g)$	[31]
I79 *	$O_3^- + O_2^+ \rightarrow O_3 + O_2$	$2.0 \cdot 10^{-13}(300/T_g)^{0.5}$	[51]
I80 *	$O_3^- + O_2^+ \rightarrow O_3 + O + O$	$1.0 \cdot 10^{-13}(300/T_g)^{0.5}$	[51]
I81 *	$O_3^- + O^+ \rightarrow O_3 + O$	$1.0 \cdot 10^{-13}(300/T_g)^{0.5}$	[31]
I82 *	$O_3^- + M \rightarrow O_3 + M + e^-$	$2.3 \cdot 10^{-17}$	[31]
I84 *	$O^- + O^+ \rightarrow O + O$	$4.0 \cdot 10^{-14}(300/T_g)^{0.43}$	[51]
I85 *	$O^- + O^+ + M \rightarrow O_2 + M$	$1.0 \cdot 10^{-37}(300/T_g)^{2.5}$	[51]
I86 *	$O^- + O_2^+ \rightarrow O_2 + O$	$2.6 \cdot 10^{-14}(300/T_g)^{0.44}$	[51]
I87 *	$O^- + O_2^+ \rightarrow O + O + O$	$4.2 \cdot 10^{-13}(300/T_g)^{0.44}$	[51]
I88 *	$O^- + O_2^+ + M \rightarrow O_3 + M$	$1.0 \cdot 10^{-37}(300/T_g)^{2.5}$	[31]
I89 *	$O^- + M \rightarrow O + M + e^-$	$4.0 \cdot 10^{-18}$	[38]
I90 *	$O_4^- + M \rightarrow O_2^- + O_2 + M$	$1.0 \cdot 10^{-16} \exp(-1044/T_g)$	[40]
I91 *	$O_4^+ + M \rightarrow O_2^+ + O_2 + M$	$3.3 \cdot 10^{-12}(300/T_g)^4 \exp(-5030/T_g)$	[40]

Table A5: The VV and VT reactions of CO_2, CO and O_2, with the corresponding rate coefficient, obtained from[6]. The anharmonicity parameter x_e is required when applying the VV and VT rate coefficient scaling laws (equations (14) and (18)).

No.	Rate coefficient (m^3/s)	$x_e(\cdot 10^{-3})$	Ref	Note
V1	$CO_2v_a + M \rightarrow CO_2 + M$	0.0	[55]	a
	$7.14 \times 10^{-14} \exp(-177\, T_g^{-1/3} + 451\, T_g^{-2/3})$			
V2a	$CO_2v_1 + M \rightarrow CO_2v_a + M$	3.7	[55]	b
	$4.25 \times 10^{-7} \exp(-407\, T_g^{-1/3} + 824\, T_g^{-2/3})$			
V2b	$CO_2v_1 + M \rightarrow CO_2v_b + M$	1.0	[55]	b
	$8.57 \times 10^{-7} \exp(-404\, T_g^{-1/3} + 1096\, T_g^{-2/3})$			
V2c	$CO_2v_1 + M \rightarrow CO_2v_c + M$	−15.6	[55]	b
	$1.43 \times 10^{-11} \exp(-252\, T_g^{-1/3} + 685\, T_g^{-2/3})$			
V3	$COv_1 + M \rightarrow CO + M$	6.13	[7]	c
	$1.0 \times 10^{-18}\, T_g \exp(-150.7\, T_g^{-1/3})$			
V4	$COv_1 + O_2 \rightarrow CO + O_2$	6.13	[55]	
	$3.19 \times 10^{-12} \exp(-289\, T_g^{-1/3})$			
V5	$O_2v_1 + M \rightarrow O_2 + M$	0.0	[55]	d
	$1.30 \times 10^{-14} \exp(-158\, T_g^{-1/3})$			
V6	$O_2v_1 + O_2 \rightarrow O_2 + O_2$	0.0	[7]	
	$1.35 \times 10^{-18}\, T_g \exp(-137.9\, T_g^{-1/3})[1 - \exp(-2273/T_g)]^{-1}$			
V7a	$CO_2v_1 + CO_2 \rightarrow CO_2v_b + CO_2v_a$	2.8	[55]	
	$1.06 \times 10^{-11} \exp(-242\, T_g^{-1/3} + 633\, T_g^{-2/3})$			
V7b	$CO_2v_1 + CO_2 \rightarrow CO_2v_a + CO_2v_b$	17.6	[55]	
	$1.06 \times 10^{-11} \exp(-242\, T_g^{-1/3} + 633\, T_g^{-2/3})$			
V8	$CO_2v_1 + CO_2 \rightarrow CO_2 + CO_2v_1$	5.25	[65]	
	$1.32 \times 10^{-16} (T_g/300)^{0.5}\, 250/T_g$			
V9	$COv_1 + CO \rightarrow CO + COv_1$	6.13	[7]	
	$3.4 \times 10^{-16} (T_g/300)^{0.5}\, (1.64 \times 10^{-6}\, T_g + 1.61/T_g)$			
V10	$CO_2v_1 + CO \rightarrow CO_2 + CO_2v_1$	5.25; 6.13	[55]	
	$4.8 \times 10^{-18} \exp(-153\, T_g^{-2/3})$			

[a] The rate coefficient is multiplied with 1.0, 0.7 and 0.7 for CO_2, CO and O_2, respectively.
[b] The rate coefficient is multiplied with 1.0, 0.3 and 0.4 for CO_2, CO and O_2, respectively.
[c] The same rate coefficient for M = CO_2 and CO.
[d] The rate coefficient is multiplied with 0.3 and 1.0 for M = CO_2 and CO, respectively.